

1
2
3
4
5
6
7
8
9
10
11
12
13
14
15
16
17
18
19
20
21
22
23
24
25
26
27

Human PDCD2L is an export substrate of CRM1 that associates with 40S ribosomal subunit precursors

Anne-Marie Landry-Voyer¹, Sarah Bilodeau¹, Danny Bergeron¹, Kiersten L. Dionne¹, Sarah A. Port², Caroline Rouleau¹, François-Michel Boisvert³, Ralph H. Kehlenbach², and François Bachand^{1,#}

¹RNA Group, Department of Biochemistry, Université de Sherbrooke, 3201 Jean-Mignault, Sherbrooke, Québec, Canada J1E 4K8.

²Department of Molecular Biology, Faculty of Medicine, GZMB, Georg-August-University Göttingen, Humboldtallee 23, 37073 Göttingen, Germany

³Department of Anatomy and Cell Biology, Université de Sherbrooke, 3201 Jean-Mignault, Sherbrooke, Québec, Canada J1E 4K8.

#Correspondence and requests for materials should be addressed to F.B. (f.bachand@usherbrooke.ca).

Abstract: 206 words

Materials & Methods: 1687 words/9516 characters

Abstract, Introduction, Results, Discussion, and figure legends: 39881 characters

Running Head: *PDCD2L contributes to 40S ribosomal subunit biogenesis*

28
29
30
31
32
33
34
35
36
37
38
39
40
41
42
43
44
45
46
47
48
49

ABSTRACT

The protein arginine methyltransferase 3 (PRMT3) forms a stable complex with the 40S ribosomal protein S2 (RPS2) and contributes to ribosome biogenesis. However, the molecular mechanism by which PRMT3 influences ribosome biogenesis and/or function still remains unclear. Using quantitative proteomics, we identified the human Programmed Cell Death 2-like (PDCD2L) as a novel PRMT3-associated protein. Our data suggest that RPS2 promotes the formation of a conserved extra-ribosomal complex with PRMT3 and PDCD2L. We also show that PDCD2L associates with 40S subunit precursors that contain a 3'-extended form of the 18S rRNA (18S-E pre-rRNA) and several pre-40S maturation factors. PDCD2L shuttles between the nucleus and cytoplasm in a CRM1-dependent manner using a leucine-rich nuclear export signal that is sufficient to direct the export of a reporter protein. Although PDCD2L is not required for the biogenesis and export of 40S ribosomal subunits, we found that *PDCD2L*-null cells accumulate free 60S ribosomal subunits, indicative of a deficiency in 40S subunit availability. Our data also indicate that PDCD2L and its paralog, PDCD2, function redundantly in 40S ribosomal subunit production. Our findings uncover the existence of an extra-ribosomal complex consisting of PDCD2L, RPS2, and PRMT3, and support a role for PDCD2L in the late maturation of 40S ribosomal subunits.

50

INTRODUCTION

51

52

53

54

55

56

57

58

59

60

61

62

63

64

65

66

67

68

69

70

71

72

73

74

75

76

77

78

79

80

81

82

83

Proliferating cells greatly rely on protein synthesis to provide a continuous source of structural and catalytic proteins to grow, duplicate, and expand. The ribosome is the evolutionarily conserved macromolecular machine responsible for protein synthesis, and consists of a ribonucleoprotein complex composed of four noncoding ribosomal RNAs (rRNAs) and ~80 ribosomal proteins (RPs) in eukaryotes. Ribosome biogenesis necessitates a major commitment in terms of cellular energy consumption, involving transcription from all three eukaryotic RNA polymerases, the spatial and temporal action of more than 300 ribosome assembly factors, and several quality control checkpoints to ensure proper ribosome assembly (1). In fact, given the substantial amount of resources invested in making ribosomes, the past few years have seen a growing body of evidence linking ribosome biogenesis to nutrient, growth factor, and stress responses (2), thereby implicating regulation of ribosome biogenesis in stem cells homeostasis (3, 4) and cancer biology (5).

In eukaryotes, ribosome biogenesis begins in the nucleolus with the synthesis of a precursor rRNA that is co-transcriptionally assembled into a large ribonucleoprotein particle (RNP) via the recruitment of specific RPs and early maturation factors (6). This large ~90S pre-ribosome complex is then rapidly converted into precursors of the 40S and 60S ribosomal subunits via a complex series of endonucleolytic and exonucleolytic RNA cleavage events (6). Pre-40S particles are rapidly exported from the nucleus and further processed in the cytoplasm, whereas maturation of the pre-60S continues in the nucleus before export to the cytoplasm. Nuclear export of pre-40S and pre-60S particles both depend on the RanGTP-binding exportin, CRM1, which recognizes a leucine-rich nuclear export signal (NES) in adaptor proteins to facilitate export from the nucleus (7). Interestingly, whereas the NES-containing adaptor Nmd3 has been shown to be essential for pre-60S export in yeast and vertebrates (8-11), the identification of a similar NES adaptor essential for pre-40S subunit export has remained elusive.

Historically, the ribosome is viewed as a generic machine that translates all mRNAs equally. However, findings in the past decade challenge this simplistic view and suggest that heterogeneity in ribosome composition may give rise to specialized ribosomes (12). One of the mechanisms proposed to promote ribosome heterogeneity is the addition of post-translational modifications to RPs. Interestingly, whereas RPs are subject to a variety of posttranslational modifications (13-15), few RP-modifying enzymes have been identified. Methylation of RPs at arginines in both the eukaryotic 40S and 60S ribosomal subunits is evolutionarily conserved (16-18) and fluctuates depending on growth conditions (19, 20). Work in the fission yeast *Schizosaccharomyces pombe* identified the first eukaryotic RP methyltransferase, PRMT3, which methylates the 40S ribosomal

Landry-Voyer et al., 2016

84 protein S2 (RPS2) (21). PRMT3 is an evolutionarily conserved cytosolic arginine methyltransferase
85 that contains a single C2H2-type zinc finger (22), which is required for interaction with RPS2 (23).
86 Arginine methylation of RPS2 was also demonstrated in human cells (24) and in *S. cerevisiae* (25),
87 indicating the existence of a conserved RP modification. Consistent with a role in ribosome
88 function, disruption of *PRMT3* results in aberrant ribosome profiles in *S. pombe* and *Arabidopsis*
89 (21, 23, 26). Furthermore, hypomorphic *PRMT3* mice and *PRMT3*-null plants show developmental
90 defects reminiscent of ribosome biogenesis mutants, including reduced embryo size and growth
91 retardation (26, 27). As yet, however, the exact role of PRMT3 in ribosome biogenesis and/or
92 ribosome function remains poorly understood.

93 Here, we used quantitative proteomics in human cells to identify novel PRMT3-associated
94 proteins. High-resolution mass spectrometry analysis of PRMT3 purifications uncovered a stable
95 complex consisting of PRMT3, RPS2, and the Programmed Cell Death 2-like (PDCD2L) protein.
96 PDCD2L belongs to a protein family that contains a TYPP (*TSR4*, *YwqG*, *PDCD2L*, and *PDCD2*)
97 domain, which has been proposed to promote protein-protein interactions based on structure
98 prediction (28). Although the *S. cerevisiae* ortholog of PDCD2L, *Trs4p*, is required for processing of
99 the 20S pre-rRNA into mature 18S rRNA (29), the functional role of human PDCD2L had remained
100 unknown. In this study, we show that a fraction of PDCD2L associates with late stage 40S
101 ribosomal subunit precursors that contain a 3'-extended form of 18S rRNA. PDCD2L contains a
102 leucine-rich NES that is both necessary and sufficient for interaction with CRM1 and
103 nucleocytoplasmic shuttling. Disruption of PDCD2L expression in human cells resulted in the
104 accumulation of free 60S ribosomal subunits, a phenotype suggestive of defects in 40S ribosomal
105 subunit availability. Our data also reveal some level of redundancy between PDCD2L and its
106 paralog, PDCD2, in 40S ribosomal subunit biogenesis. Our findings uncover the existence of an
107 extra-ribosomal complex consisting of PDCD2L, RPS2, and PRMT3, and support a role for
108 PDCD2L in the late maturation of 40S ribosomal subunits.
109

110

MATERIALS AND METHODS

111 **Cell culture.** HEK 293, U-2 OS, and HeLa cells were grown in Dulbecco's modified Eagle's
112 medium (DMEM) supplemented with 10% of tetracycline-free fetal bovin serum (FBS). Inducible
113 expression of GFP, GFP-PRMT3, GFP-PDCD2L, GFP-PDCD2L^{NE5mut}, GFP-PABPN1, Flag-
114 PDCD2L, and Flag-PABPN1 was achieved by site-directed recombination using the Flp-*FRT*
115 system in HEK 293-FT and U-2 OS-FT cells, as previously described (30). Induction of GFP- and
116 Flag-tagged proteins was achieved with 500 ng/mL of doxycycline for 20h-72h. siRNAs were
117 transfected with Lipofectamine 2000 at a final concentration of 25nM (siControl and siPDCD2L) or
118 32 nM (siBystin and siRPS2) for 72 h.

119

120 **Generation of *PDCD2L*-null cells using the CRISPR-Cas9 system.** For deletion of *PDCD2L* in
121 HeLa cells, 2 gRNAs, the Cas9 nickase and a template DNA were used. The following gRNAs, A)
122 5'-CGTGCACCGGCGCATCTCGAAGG-3' and B) 5'-TGCCTGGACTGCTAGCAAGCTGG-3', were
123 designed via the CRISPR Desing webtool available at crispr.mit.edu. These sequences were
124 inserted in the pSpCas9n(BB)-2A-GFP vector (Addgene) as previously described (31). For the
125 construction of the template DNA construct containing the puromycin resistance gene (Puromycin
126 N-acetyl-transferase - PAC) under the control of the CMV promoter flanked by two *PDCD2L*
127 homology regions, pEGFP-C1 (Clontech) was used as the backbone vector. The PAC sequence
128 was amplified from pTRIPZ (GE Dharmacon) and the CMV promoter and immediate-early
129 enhancer sequences were amplified from pEGFP-C1 (Clontech). *PDCD2L* homology sequences
130 were amplified from HeLa genomic DNA. For the 5' *PDCD2L* homology arm, a 791 base pair
131 sequence ending at the nucleotide before the gRNA-A was amplified. For the 3' *PDCD2L*
132 homology arm, a 784 base pair sequence starting at the nucleotide after the gRNA-B was
133 amplified. Gibson assembly was used to insert the homology arms into the backbone vector. The
134 PAC and CMV promoter sequences were joined by PCR fusion and inserted between the
135 homology arms using *Bgl*III and *Not*I digestions.

136 HeLa cells were seeded in a 15-cm plate. The next day, cells were transfected with 10 µg of
137 pSpCas9n(BB)-2A-GFP-gRNA-A, 10 µg of pSpCas9n(BB)-2A-GFP-gRNA-B, and 20 µg of the
138 linearized DNA template using 80 µL of Lipofectamine 2000 (Life Technologies). 48h post-
139 transfection, positive cells were selected by the addition of 2 µg/mL of puromycin (Wisent) to the
140 cell culture medium. Following the visual detection of puromycin-resistant colonies, cells were
141 detached, counted, and diluted sufficiently to obtain 1 cell/well in a 96-well plate. Following cellular
142 expansion of individual clones in puromycin-supplemented media, the cells were divided into two
143 24-well plates: one was used for screening by Western blot and the other was used for cell

Landry-Voyer et al., 2016

144 maintenance. In total, five independent *PDCD2L*-null clones were frozen and kept in liquid
145 nitrogen. The inactivation of *PDCD2L* alleles was confirmed by DNA sequencing and western
146 blotting.

147

148 **SILAC and label-free purifications.** For SILAC experiments, proteins were labeled with stable
149 isotopes of arginine and lysine in cell culture, as previously described (32). Briefly, HEK 293-FT
150 cells expressing GFP- or Flag-tagged versions of proteins were grown in media containing labeled
151 amino acids (Cambridge Isotope Laboratories). 24-48h after induction with doxycycline, cells were
152 collected in lysis buffer (50mM Tris-HCL, pH 7.5, 150 mM NaCl, 0.1% Triton X-100, 10% glycerol,
153 2 mM MgCl₂, 1 mM dithiothreitol [DTT] and 1X Complete protease inhibitor cocktail [Roche]) and
154 incubated at 4°C for 20 min. Lysates were centrifuged for 10 min at 13,000 × *g* at 4°C and equal
155 amount of proteins were incubated with GFP-trap agarose beads from ChromaTek (Martinsried,
156 Germany) or Anti-Flag M2 affinity gel (Sigma Aldrich) for 3 h at 4°C. Beads were then washed 5
157 times with lysis buffer and proteins were subjected to two rounds of elution by adding 100µl of
158 denaturing buffer (50 mM Tris-HCl pH 6.8, 2% SDS, 0.1 mM DTT) for 10 min at 90°C. Eluates
159 were concentrated by speedvac and resuspended in reducing buffer (125 mM Tris-HCl pH 8.0,
160 1.25% SDS, 37.5% glycerol, 60 mM DTT, 0.025% bromophenol blue). Gel electrophoresis, in-gel
161 digestions, LC-MS/MS, and analysis of SILAC ratios were performed as described previously (32).

162

163 **Protein analysis and antibodies.** Proteins were separated by SDS-PAGE, transferred to
164 nitrocellulose membranes, and analyzed by immunoblotting using the following primary antibodies:
165 anti-PABPN1 (Epitomics); anti-tubulin, anti-actin, and anti-Flag (T5168, A5441 and F1804,
166 respectively; Sigma-Aldrich); anti-PRMT3 (A302-526A; Bethyl); anti-PDCD2L (A303-783A; Bethyl);
167 anti-hRRP12, anti-PNO1, and anti-Bystin (sc-139043, sc-133263 and sc-271722, respectively;
168 Santa Cruz Biotechnology); anti-hLTV1 (ab122100; Abcam); anti-RPL17 (GTX111934; GeneTex),
169 and anti-RPS2 (a generous gift from Dr. Mark Bedford). Membranes were then probed with either a
170 donkey anti-rabbit antibody conjugated to IRDye 800CW (926-32213; LI-COR) or a goat anti-
171 mouse antibody conjugated to Alexa Fluor 680 (A-21057; Life Technologies). Proteins detection
172 was performed using an Odyssey infrared imaging system (LI-COR).

173

174 **Yeast two-hybrid assays.** *PRMT3*, *RPS2* and *PDCD2L* cDNAs were cloned in pVP16 and
175 pLexNA plasmids and transformed in *Saccharomyces cerevisiae* strain L40. Levels of β-
176 galactosidase activity were measured by liquid assays within the linear response range, as
177 previously described (33).

178

179 **Sucrose gradient analysis.** To analyze the cosedimentation of PDCD2L with ribosomal particles,
180 sucrose gradient centrifugation was performed as previously described (21). Briefly, cells were
181 washed with PBS, centrifuged, resuspended, and incubated in lysis buffer (10 mM Tris-HCL, pH
182 7.4, 100 mM KCl, 10 mM MgCl₂, 1 mM DTT, 1% Triton X-100, Complete protease inhibitor cocktail
183 [Roche], 40U/mL RNase OUT [Life Technologies] and 50 µg/mL cycloheximide [Sigma Aldrich]) for
184 20 min at 4°C. Following clarification of the lysate by centrifugation at 13,000 rpm for 10 min at
185 4°C, 7-10 mg of total protein was loaded onto a 10-45% sucrose gradient and centrifuged for 6 h at
186 40,000 rpm at 4°C in a SW41 rotor (Beckman Coulter). The gradient was then fractionated by
187 upward displacement with 55% (w/v) sucrose using a gradient fractionator (Brandel Inc.)
188 connected to a UA-6 UV monitor (Teledyne Isco) for continuous measurement of the absorbance
189 at 254 nm. 0.6-ml fractions were collected, proteins were precipitated with TCA (15% final), and
190 analyzed by western blotting.

191 For ribosome distribution profiles, cycloheximide-treated cells were washed twice with PBS
192 and lysis buffer was added directly in the 15-cm dishes. Cells were scraped, incubated 20 min at
193 4°C, and centrifuged. Five percent of the supernatant was kept for western analysis and the
194 remainder (3,5 mg of total protein) was loaded onto a 5-50% sucrose gradient and centrifuged for
195 3h at 40,000 rpm. 40S, 60S, and 80S subunits curves were reproduced in Excel and the area
196 under the curve was calculated using the rectangle method.

197

198 **RNA analysis.** Total RNA was prepared using TRIzol (Life Technologies) and pre-rRNA species
199 were analyzed by Northern blotting, as previously described (34), with the following modifications:
200 4 µg/well of total RNA, mixed with 5 volumes of loading dye (10mM EDTA, 60% glycerol, 0.04%
201 bromophenol blue), were loaded on a 0.8% denaturing agarose gel (0.8% agarose, 20 mM MOPS,
202 5 mM sodium acetate, 1 mM EDTA, 6.3% formaldehyde) and run in MOPS buffer (20 mM, 5 mM
203 sodium acetate, 1 mM EDTA) at 110V. Northern blots were hybridized using ³²P-labeled probes
204 (5'-ITS1: 5'-CCTCGCCCTCCGGGCTCCGTTAATGATC-3', 18S: 5'-
205 TTTACTTCCTCTAGATAGTCAAGTTCGACC-3' and 28S: 5'-
206 CCCGTTCCCTTGGCTGTGGTTTCGCT-3'). Signals were detected and quantified using a
207 Typhoon Trio instrument.

208

209 **RNA coimmunoprecipitation (RIP) assay.** A 15-cm dish of HEK 293-FT conditionally expressing
210 Flag-PDCD2L or Flag-PABPN1 were induced using doxycycline for 72h. Cells were washed twice
211 with PBS and 5% of cells were kept for total RNA extraction (input fraction). Cells were then

Landry-Voyer et al., 2016

212 resuspended in lysis buffer (50mM Tris-HCL, pH 7.5, 150 mM NaCl, 0.1% Triton X-100, 10%
213 glycerol, 2 mM MgCl₂, 1 mM DTT, Complete protease inhibitor cocktail [Roche] and 40U/mL
214 RNase OUT [Life Technologies]) and incubated 20 min at 4°C. Lysate was centrifuged at 13,000
215 rpm for 10 min at 4°C and 5% of the lysate was kept for protein analysis. The remainder of the
216 lysate was incubated with anti-Flag M2 affinity gel (Sigma Aldrich) for 3 h at 4°C. The beads were
217 washed 5 times with lysis buffer and 10% of the beads were kept for protein analysis. RNA was
218 extracted from the remainder of the beads using TRIzol reagent (Life Technologies) and analyzed
219 by Northern blotting.

220

221 **rRNA pulse-chase assays.** Pulse-chase analyses of pre-rRNA processing were performed based
222 on a previously described method (35), but with some modifications. Briefly, wild-type and
223 *PDCD2L*-null cells were incubated in serum-free and methionine-free medium for 30 min, after
224 which the cells were pulsed for 30 min using the same medium, but supplemented with 25μCi of L-
225 [*methyl*-³H]methionine (1 μCi/ml). The cells were then rinsed with regular medium and chased in
226 complete DMEM for the indicated time points. Cells were rinsed with ice-cold PBS and
227 resuspended in 500 μl of Trizol reagent for RNA extractions. 15,000-20,000 c.p.m. of radioactivity
228 were resolved on 1.25% agarose-formaldehyde gels. RNAs were then transferred to Hybond-N+
229 (GE Healthcare) membranes, UV cross-linked, and exposed to film for 3–4 weeks at –80°C.

230

231 **Microscopy.** Leptomycin B (LMB) was purchased from Sigma Aldrich and used at a final
232 concentration of 10 nM in 70% methanol. Visual analysis of GFP-tagged proteins in human cells
233 was as previously described (36). U-2 OS cells were washed twice with PBS, fixed with 4%
234 paraformaldehyde for 10 min at room temperature, and washed twice again with PBS. Fixed cells
235 were permeabilized using a 0,2% triton X-100/PBS solution for 10 min and washed 3 times with
236 PBS. For Fig. 5, cells were equilibrated for 20 min in PBS/1% BSA followed by a 1 h incubation
237 with primary antibody dilution in PBS/1% BSA (anti-fibrillarin 1/400 [Cell Signaling Technology]).
238 Cells were washed 3 times with PBS/1% BSA and incubated with a secondary antibody dilution
239 (rabbit Alexa Fluor 568 [Invitrogen], 1/1000 in PBS/1% BSA) for 1 h. After 3 washes, coverslips
240 were mounted on a slide with SlowFade Gold Antifade solution (Life Technologies). Images were
241 captured by Zeiss Axio Observer microscope with either a 63X or 100X oil objective.

242

243 **CRM1-binding assay.** The flow cytometry-based *in vitro* binding assays were performed as
244 previously described (37). *PDCD2L* cDNA was transferred into pDEST15 plasmid using LR
245 Clonase II (Life Technologies). To obtain pDEST15-PDCD2L_{NESmut}, we substituted leu162, leu165,

Landry-Voyer et al., 2016

246 and leu167 for alanine residues by site-directed mutagenesis. GST alone, GST-PDCD2L, and
247 GST-PDCD2L_{NESmut} proteins were produced in *E. coli* BL21 cells and purified using glutathione
248 sepharose beads. Nine pmol of Cy3-labeled CRM1 alone or in presence of 180 pmol RanQ69L-
249 GTP and 70 pmol Nup214 (amino acids 1916-2033) were used in the binding assays.
250

251

RESULTS

252 Identification of PDCD2L as a new PRMT3-associated protein

253 We and others have previously reported the identification of a complex between PRMT3 and the
254 40S ribosomal protein S2 (RPS2) (21, 24). However, with the exception of RPS2, the protein
255 interaction network of PRMT3 has remained largely unknown. To investigate the network of
256 PRMT3-associated proteins, we generated a Flp-In T-Rex HEK 293 cell line expressing a
257 tetracycline-inducible and N-terminally GFP-tagged version of PRMT3. Specific PRMT3 interaction
258 partners were determined using the stable isotope labeling in cell culture (SILAC) methodology
259 (38), followed by GFP-PRMT3 purification and high-resolution mass spectrometry (MS). The
260 presence of the GFP-PRMT3 bait protein in the eluate was confirmed by western blotting before
261 MS analysis.

262 The SILAC-coupled MS approach classifies interactions by specificity (ratio of peptide
263 intensities between the GFP-PRMT3 purification and a control purification) and protein abundance,
264 as estimated from the sum of peptide signal intensities of a given protein normalized to its
265 molecular mass (**Fig. 1A**). As expected, RPS2 was the strongest PRMT3-associated protein
266 identified by SILAC, detected at high levels in the PRMT3 pull-down. In total, 151 proteins showed
267 at least 2-fold enrichment in the SILAC ratio in the GFP-PRMT3 purification relative to the control
268 (**Table S1** and **Fig. 1A**). Notably, besides RPS2, the programmed cell death 2-like (PDCD2L)
269 protein was among the strongest PRMT3-associated proteins, showing a robust SILAC ratio and
270 high abundance (**Fig. 1A** and **Table S1**). A reciprocal immunoprecipitation assay validated the
271 PRMT3-PDCD2L association, as PRMT3, but not actin, was detected in the eluate of an anti-Flag
272 purification of Flag-PDCD2L (**Fig. 1B**, lane 8). In contrast, PRMT3 was not detected in eluates of
273 control purifications (**Fig. 1B**, lanes 5-7). Importantly, we could show that immunoprecipitation of
274 endogenous PRMT3 copurified endogenous PDCD2L and RPS2, whereas PDCD2L and RPS2
275 were not detected in a control immunoprecipitation (**Fig. 1C**, lanes 2-3). As an additional control,
276 immunoprecipitation of endogenous PRMT3 using extracts prepared from *PDCD2L*-null cells
277 (using CRISPR/Cas9-mediated genomic targeting, see *Methods* section) did not detect PDCD2L;
278 yet, RPS2 was still copurified with PRMT3 (**Fig. 1C**, lane 4). Consistent with this, the distribution of
279 endogenous PRMT3 across a density gradient was not altered by a deficiency in PDCD2L (**Fig.**
280 **S1**). Together, these results uncover PDCD2L as a new PRMT3-associated protein and indicate
281 that PDCD2L is not required for the association between PRMT3 and RPS2.

282

283 RPS2 is required for the association between PRMT3 and PDCD2L

284 The predicted homolog of PDCD2L in *Drosophila*, TRUS (CG5333), was previously identified as an
285 RPS2-interacting protein using a high-throughput two-hybrid screening approach (39). To test
286 whether PDCD2L associates with RPS2 in human cells, we investigated the presence of RPS2 in
287 immunoprecipitates of Flag-PDCD2L. As shown in **Fig. 2A**, endogenous RPS2 and PRMT3 were
288 both detected after the purification of Flag-tagged PDCD2L (lane 4), but not in the purification of a
289 control Flag-tagged protein (lane 3). We next analyzed the association between human RPS2,
290 PRMT3, and PDCD2L using the yeast two-hybrid system. We found that RPS2 strongly interacts
291 with both PDCD2L (**Fig. 2B**, panel i) and PRMT3 (**Fig. 2B**, panel ii). Interestingly, the interaction
292 between PRMT3 and PDCD2L was roughly 5 times weaker than the interaction between PRMT3
293 and RPS2 (**Fig. 2B**, panel ii), suggesting that RPS2 may promote and/or stabilize the association
294 between PRMT3 and PDCD2L.

295 To test the possibility that RPS2 bridges the association between PRMT3 and PDCD2L, we
296 analyzed the effect of depleting RPS2 on the association between PRMT3 and PDCD2L. To this
297 end, cells that stably expressed GFP-PRMT3 and a control GFP-tagged protein were treated with
298 either RPS2-specific or control non-target siRNAs. RNAi-mediated depletion of endogenous RPS2
299 generally resulted in a 50% knockdown efficiency; yet, total levels of PDCD2L and GFP-PRMT3
300 were not affected by the depletion of RPS2 (**Fig. 2C**, compare lane 3 to lanes 1-2). Notably,
301 purification of GFP-PRMT3 from RPS2-depleted cells showed a significant decrease in the
302 recovery of PDCD2L as compared to purification of GFP-PRMT3 prepared from cells treated with
303 control siRNAs (**Fig. 2C**, compare lanes 5-6; quantification in **Fig. 2D**). We also examined whether
304 the association between RPS2 and PDCD2L in human cells required the presence of PRMT3. As
305 shown in **Fig. 2E**, depletion of PRMT3 reduced the levels of RPS2 copurified with PDCD2L
306 (compare lanes 7-8). Together, these data suggest that RPS2 and PRMT3 are both required for
307 the formation of a stable PRMT3-Rps2-PDCD2L complex.

308

309 **PDCD2L associates with 40S ribosomal subunit precursors**

310 PDCD2L exhibits sequence homology to budding yeast Tsr4p, a protein identified in a genetic
311 screen for factors required for the processing of the 20S rRNA precursor (29), which gives rise to
312 the mature 18S rRNA of the 40S ribosomal subunit. As yet, however, a molecular function for
313 human PDCD2L has remained unknown. To begin to explore the functional role of human
314 PDCD2L, we used quantitative proteomics to define the protein-protein interaction network of
315 PDCD2L via SILAC. As for PRMT3, we generated a HEK293 cell line conditionally expressing a
316 tetracycline-inducible and GFP-tagged version of PDCD2L. The analysis of PDCD2L-associated
317 proteins identified by SILAC-coupled MS is presented in **Figure 3A**. In total, 25 proteins were

318 copurified with PDCD2L with a SILAC enrichment ratio >2.0 and a minimum of two detectable
319 peptides (see **Table S2**). Notably, RPS2 and PRMT3 were the strongest interaction partners of
320 PDCD2L, showing high specificity and peptide intensity (**Fig. 3A**), suggesting the existence of a
321 stable PDCD2L-RPS2-PRMT3 complex. The purification of PDCD2L also recovered several
322 factors that have been shown to be pre-ribosomal factors composing the pre-40S particle or are
323 yeast homologs of known pre-40S components (40-42): hRRP12, Bystin/ENP1, C21orf70, PNO1,
324 hLTV1, and NOC4L (**Fig. 3A** and **Table S2**). Validation experiments confirmed that the enrichment
325 of 40S pre-ribosomal factors in the GFP-PDCD2L SILAC experiment was not dependent of the use
326 of a GFP fusion protein, as a Flag-tagged version of PDCD2L specifically recovered hRRP12,
327 hLTV1, and PNO1 (**Fig. 3B**). Furthermore, analysis of the SILAC/MS data revealed a significant
328 enrichment of ribosomal proteins from the small subunit compared to the large ribosomal subunit
329 (**Fig. S2**). These results suggest that a fraction of PDCD2L is associated to pre-40S particles.

330 We next used sucrose gradient coupled to velocity sedimentation to examine the
331 distribution of endogenous PDCD2L relative to known 40S maturation factors. As shown in **Fig.**
332 **3C**, the majority of PDCD2L was present in the low-density fractions, steadily decreasing from
333 fractions 3-7. Notably, a fraction of PDCD2L clearly co-sedimented with free 40S subunits/pre-40S
334 particles, as demonstrated by the increased levels of PDCD2L detected in fractions 9-10, which
335 are enriched in hLTV1, hRRP12, and RPS2. Fractions corresponding to free 60S, 80S
336 monosomes, and polyribosomes showed barely detectable levels of PDCD2L (**Fig. 3C**, fractions
337 11-12 and data not shown).

338 The aforementioned results suggest that a fraction of PDCD2L physically associates with
339 immature pre-40S particles and/or mature 40S ribosomal subunits. To clarify the nature of the 40S
340 particle associated with PDCD2L, we analyzed the type of rRNA associated with PDCD2L using
341 RNA co-immunoprecipitation (RIP) assays. Two major forms of 3'-extended 18S rRNA precursors
342 are associated with pre-40S particles in mammalian cells (see **Fig. 3D**): the 21S pre-rRNA that is
343 found in the nucleus and the 18S-E pre-rRNA that can be both in the nucleus and the cytoplasm
344 (43). Northern blot analysis of RNAs prepared from PDCD2L immunoprecipitates using a probe
345 complementary to internal transcribed spacer 1 (ITS1) sequences (**Fig. 3D**, red probe) revealed a
346 robust enrichment of the 18S-E rRNA precursor relative to the control purification (**Fig. 3E**,
347 compare lanes 3-4; quantification in **Fig. 3F**). A slight enrichment (1.5-2-fold) in 21S pre-rRNA was
348 also detected after a long exposure (data not shown), but was substantially less compared to the
349 marked enrichment of 18S-E pre-rRNA (**Fig. 3F**). In contrast, similar levels of mature 18S rRNA
350 were detected between PDCD2L and control immunoprecipitates (**Fig. 3E**). Taken together, the
351 data presented in Figure 3 indicate that PDCD2L associates with pre-40S particles.

352

353 **PDCD2L shuttles between nucleus and cytoplasm and interacts directly with CRM1**

354 Recent studies aimed at identifying shuttling substrates of CRM1, the major transport receptor for
355 export of proteins and RNPs from the nucleus, have identified peptides corresponding to
356 endogenous PDCD2L (44, 45). To validate that PDCD2L is exported from the nucleus in a CRM1-
357 dependent manner, we analyzed the localization of GFP-PDCD2L after incubation with the CRM1
358 inhibitor, leptomycin B (LMB) (46). Whereas GFP-PDCD2L mainly localized to the cytoplasm in the
359 absence of LMB (**Fig. 4A**, panels a-c), the majority of cells displayed PDCD2L localization
360 throughout the nucleus after LMB treatment (**Fig. 4A**, panels d-f). Notably, most cells showed
361 PDCD2L accumulation in the nucleus after only 40 min of LMB treatment (**Fig. S3**). In contrast,
362 PRMT3 did not show CRM1-dependent shuttling in U-2 OS cells, as the cytoplasmic localization of
363 GFP-PRMT3 was not affected by the inhibition of CRM1 by LMB (**Fig. 4A**, panels g-l).

364 The rapid retention of PDCD2L in the nucleus after LMB treatment suggested that PDCD2L
365 might be a direct substrate of CRM1-mediated export. We therefore analyzed the amino acid
366 sequence of PDCD2L using computer algorithms (47, 48) to predict the presence of a leucine-rich
367 nuclear export signal (NES), which is recognized by CRM1 (49). Notably, both prediction tools
368 identified a putative leucine-rich NES between amino acid 162 and 167 of human PDCD2L, a motif
369 that appears to have been conserved in diverse PDCD2L homologs (**Fig. 4B**). To test the
370 functional importance of this motif for PDCD2L nucleocytoplasmic shuttling, we substituted leu162,
371 leu165, and leu167 for alanine residues (PDCD2L_{NESmut}). The triple alanine substitution did not
372 disrupt the folding of PDCD2L, as wild-type and NES mutant versions of PDCD2L recovered
373 similar levels of RPS2 and PRMT3 after affinity purification (**Fig. S4**). However, in contrast to wild-
374 type PDCD2L, the NES mutant version was completely retained in the nucleus (**Fig. 4C**, compare
375 panels a and d). We also addressed whether the NES of PDCD2L could promote CRM1-
376 dependent nuclear export of a GFP reporter, which predominantly localizes to the nucleus at
377 steady state (**Fig. 4D**, panel a). We thus fused 28 amino acids (aa 153-181) of PDCD2L containing
378 either wild-type or mutant versions of the NES to the C-terminus of GFP (see **Fig. 4E**). Amino
379 acids 153-181 of PDCD2L were sufficient to stimulate export of the GFP reporter to the cytoplasm
380 (**Fig. 4D**, compare panels a and g). Nuclear export of the GFP-NES-PDCD2L reporter was
381 dependent on CRM1, as it accumulated in the nucleus after LMB treatment (**Fig. 4D**, compare
382 panels g and j). Importantly, the GFP reporter fused to the mutant version of the PDCD2L NES
383 remained primarily localized to the nucleus (**Fig. 4D**, panel m). We therefore conclude that the
384 PDCD2L NES is necessary and sufficient for CRM1-dependent nuclear export.

385 Next, we examined whether the NES of PDCD2L can mediate a direct interaction with
386 CRM1. To this end, we performed flow cytometry-based *in vitro* binding assays using fluorescently-
387 labeled recombinant CRM1 (37) together with recombinant versions of wild-type and mutant GST-
388 PDCD2L. Bindings assays were performed in the absence and presence of RanQ69L-GTP and a
389 fragment of Nup214, which stabilize the interaction between CRM1 and its substrates (37). A GST-
390 tagged version of HIV-1 Rev, which contains a leucine-rich NES (50), was used as a positive
391 control and bound to CRM1 in a RanGTP-dependent manner, whereas GST alone did not (**Fig.**
392 **4F**). Notably, direct binding between CRM1 and PDCD2L was observed, but was significantly
393 reduced when the NES mutant version of PDCD2L was analyzed (**Fig. 4F**). These results indicate
394 that PDCD2L is a nucleocytoplasmic shuttling protein that is an export substrate of CRM1.

395

396 **PDCD2L transits through the nucleolus**

397 Although PDCD2L predominantly localizes to the cytoplasm at steady state, analysis of higher
398 magnification images showed punctate nuclear signals that were reminiscent of nucleolar staining
399 (**Fig. 5**, panel g), which are sites of ribosome biogenesis. To test the possibility that the punctate
400 nuclear staining of PDCD2L corresponded to nucleoli, we combined GFP-PDCD2L localization
401 with an immunostaining procedure for endogenous fibrillarin, which is a nucleolar marker protein
402 (**Fig. 5**, panel d). Comparison of the different staining methods showed that GFP-PDCD2L was
403 concentrated in nuclear regions that coincided with anti-fibrillarin staining (**Fig. 5**, panels d, g, and
404 j). The observation that GFP-PDCD2L localizes to nucleoli is consistent with proteomic studies that
405 found PDCD2L as part of the nucleolar proteome (51). Interestingly, the GFP-PDCD2L nucleolar
406 signal increased shortly after LMB treatment (**Fig. 5**, panel h), but was gradually lost over time
407 (**Fig. 5**, panel i). These results suggest that PDCD2L transits through the nucleolus before it is
408 exported to the cytoplasm.

409

410 **Deletion of *PDCD2L* results in the accumulation of free 60S ribosomal subunits**

411 Our results showing that PDCD2L associates with factors involved in late stages of 40S ribosomal
412 subunit maturation (**Fig. 3A-3B**), copurifies with pre-40S particles (**Fig. 3C-3F**), and shuttles
413 between the nucleus and cytoplasm using a leucine-rich NES (**Fig. 4**) suggested that PDCD2L
414 could act as an adapter protein for CRM1-mediated export of pre-40S particles. We therefore
415 performed RNAi experiments to examine the effect of PDCD2L depletion on pre-40S export from
416 the nucleus. Two independent assays were used to monitor pre-40S localization: (i) fluorescent *in*
417 situ hybridization (FISH) using an ITS1-specific probe to detect accumulation of 18S-E pre-rRNA in
418 the nucleoplasm and/or reduction in the cytoplasm; and (ii) immunostaining of the late pre-40S-

419 associated factor, hLTV1, for nuclear accumulation in PDCD2L-deficient cells. Whereas CRM1
420 inhibition using LMB showed the expected accumulation of 18S-E pre-rRNA and hLTV1 in the
421 nucleoplasm, PDCD2L depletion did not result in a detectable change in pre-40S subcellular
422 localization (data not shown). We also analyzed the levels of 40S pre-rRNA species by northern
423 blotting using probes complementary to ITS1-specific sequences. Control experiments targeting
424 the pre-40S maturation factor, Bystin (**Fig. 6A**, lane 3), resulted in the accumulation of 21S pre-
425 rRNA together with reduced levels of mature 18S rRNA (**Fig. 6B**, compare lane 3 to lane 1; **Fig.**
426 **6C-6D** for quantifications), consistent with previous observations (34). In contrast, despite efficient
427 PDCD2L depletion (**Fig. 6A**, lane 2), a deficiency in PDCD2L did not result in the accumulation of
428 21S and 18S-E rRNA precursors (**Fig. 6B-6D**). To test the possibility that residual levels of
429 PDCD2L after RNAi-mediated depletion could be sufficient to promote pre-40S nuclear export, we
430 used CRISPR/Cas9-mediated genomic targeting in HeLa cells to generate multi-allelic mutations in
431 *PDCD2L*, resulting in cells with undetectable levels of PDCD2L protein (**Fig. S5**). Consistent with
432 siRNA-mediated depletions of PDCD2L, *PDCD2L*-null cells did not reveal major defects in the
433 maturation of pre-40S particles as determined by Northern analysis (data not shown) and rRNA
434 pulse-chase assays (**Fig. S6**). However, the analysis of ribosome distribution by sucrose gradient
435 centrifugation showed the accumulation of free 60S ribosomal subunits using two independent
436 knockout clones of *PDCD2L* (**Fig. 7A**, compare 1A3 and 3B2 to WT); yet, the levels of free 40S
437 ribosomal subunits did not appear to change between PDCD2L knockout and control parental cells
438 (**Fig. 7A**). The accumulation of free 60S subunits in *PDCD2L*-null cells significantly altered the
439 stoichiometry between free 40S and 60S ribosomal subunits (**Fig. 7B**), but not the overall content
440 of 80S monosomes and polyribosomes (**Fig. 7A**).

441 To ensure that the accumulation of free 60S ribosomal subunit in PDCD2L knock-out cells was
442 indeed caused by a deficiency in PDCD2L, we performed rescue experiments using a Flag-tagged
443 version of PDCD2L. Expression of wild-type PDCD2L restored the increased levels of free 60S
444 ribosomal subunits detected in *PDCD2L*-null cells (**Fig. 7C**, compare panels 2 and 3), resulting in
445 levels of free 60S similar to parental control cells (**Fig. 7C**, panel 1). In contrast, *PDCD2L*-null cells
446 transfected with the empty vector control showed the expected accumulation of free 60S ribosomal
447 subunits (**Fig. 7C**, panel 2).

448

449 **PDCD2L and its paralog, PDCD2, function redundantly in ribosome biogenesis**

450 In addition to PDCD2L, our analysis of PRMT3-associated proteins also identified PDCD2 (see
451 Table S1), a paralog of PDCD2L that is 30% identical (52% similar) to human PDCD2L. Based on
452 sequence analysis, PDCD2 is thought to have arose from duplication of the *PDCD2L* gene prior to

Landry-Voyer et al., 2016

453 the divergence of animals, fungi, and plants from a common ancestor (28). Interestingly, it was
454 recently found that the *Drosophila* homolog of PDCD2, Zfrp8, interacts with Rps2 (52). Considering
455 the seemingly similar functions ascribed to human PDCD2L and *Drosophila* PDCD2 (Zfrp8), we
456 examined whether human PDCD2 contributes to ribosome biogenesis and potentially acts
457 redundantly to PDCD2L. As shown in **Fig. 8A**, PDCD2 was efficiently depleted from the parental
458 HeLa cell line (lane 2) as well as from *PDCD2L*-null cells (lane 4). Analysis of ribosome production
459 using extracts prepared from PDCD2-depleted cells showed reduced levels of free 40S ribosomal
460 subunits together with increased levels of free 60S subunits (**Fig. 8B**, compare panels a-b),
461 affecting the levels of 80S monosomes, but not polysomes level. We next examined the effect of
462 depleting PDCD2 in *PDCD2L*-null cells to characterize the functional relationship between PDCD2
463 and PDCD2L. Notably, the combined deficiency of both PDCD2 and PDCD2L resulted in a
464 synergistic increase in the 60S:40S free subunit ratio relative to either PDCD2 or PDCD2L single
465 depletion (**Fig. 8B**, compare panel d to panels b-c). Cells deficient for both PDCD2 and PDCD2L
466 also showed reduced levels of 80S monosomes as well as a reduction in the amplitude of
467 polysomes peaks relative to PDCD2 and PDCD2L single depletions (**Fig. 8B**). The functional
468 relationship between PDCD2 and PDCD2L in 40S ribosomal subunit biogenesis demonstrated by
469 sucrose gradient analyses was supported by Northern blot assays of pre-rRNA processing using
470 an ITS1-specific probe. Accordingly, cells deficient for PDCD2 showed accumulation of 18S-E and
471 21S pre-rRNAs (**Fig. 8C**, lane 2), an accumulation that was further increased by the co-depletion of
472 both PDCD2 and PDCD2L (**Fig. 8C**, lane 4; quantifications in **Fig. 8D-8E**). Cells deficient for both
473 PDCD2 and PDCD2L also showed reduced levels of mature 18S rRNA (**Fig. 8C**, lanes 4). From
474 these results, we conclude that PDCD2 is important for optimal 40S ribosomal subunit production
475 and that PDCD2 and PDCD2L have partially overlapping functions in 40S biogenesis.

476 To further investigate the functional relationship between PDCD2L and PDCD2, we used
477 SILAC-based quantitative proteomics to determine the protein interaction network of human
478 PDCD2. Using a stable cell line conditionally expressing a GFP-tagged version of PDCD2, we
479 identified 80 proteins that copurified with PDCD2 with a SILAC enrichment ratio >2.0 and a
480 minimum of two detectable peptides (see **Table S3**). As for PDCD2L, RPS2 and PRMT3 were the
481 strongest interaction partners of PDCD2, showing robust peptide intensities (**Fig. 8F**). Interestingly,
482 despite of the fact that both PDCD2 and PDCD2L associated with the RPS2-PRMT3 duo, PDCD2L
483 peptides were not detected in the PDCD2 purification, and reciprocally, PDCD2 was not identified
484 as a PDCD2L-associated protein. Furthermore, the mass spectrometry analysis of PDCD2-
485 associated proteins did not recover pre-ribosomal maturation factors, which is in striking contrast to
486 PDCD2L for which several pre-40S components were identified and validated (**Fig. 3**). Taken

Landry-Voyer et al., 2016

487 together, our data suggest some level of redundancy between PDCD2L and PDCD2 paralogs in
488 40S ribosomal subunit biogenesis, contributing to parallel pathways that would converge to the
489 RPS2-PRMT3 complex.
490

491

492

DISCUSSION

493 In this study, we report that human PDCD2L forms a stable complex with RPS2 and the protein
494 arginine methyltransferase, PRMT3. Our results also indicate that PDCD2L is a nucleocytoplasmic
495 shuttling protein that associates with pre-40S particles and that disruption of PDCD2L expression
496 leads to the accumulation of free 60S ribosomal subunits, findings that suggest a role for PDCD2L
497 in the supply of mature 40S ribosomal subunits.

498

RPS2 forms an extra-ribosomal complex with PRMT3 and PDCD2L

500 Our analysis of PRMT3- and PDCD2L-associated proteins using SILAC-based proteomics
501 revealed that both PRMT3 and PDCD2L strongly associate with RPS2. Notably, levels of RPS2
502 were 1000-times and 200-times the levels of the next most abundant ribosomal protein detected in
503 the PRMT3 and PDCD2L purifications, respectively. Consistent with our results, a recent study
504 using high-throughput affinity purification coupled to mass spectrometry detection also supports the
505 existence of a stable PRMT3-RPS2-PDCD2L complex in human cells (53). The robust levels of
506 RPS2 detected after the purification of human PRMT3 (**Fig. 1A**) is also consistent with data in
507 fission yeast, where RPS2 was the predominant ribosomal protein identified after purification of *S.*
508 *pombe* Rmt3 (21). In addition, a two-hybrid-based interaction map of the *Drosophila* proteome (39)
509 reports interactions between SOP and TRUS (RPS2 and PDCD2L) as well as between SOP and
510 ART3 (RPS2 and PRMT3), but not between ART3 and TRUS (PRMT3 and PDCD2L). These
511 observations are consistent with our data (**Fig. 2C-2D**) indicating that RPS2 is required for the
512 copurification of PDCD2L and PRMT3. Collectively, the aforementioned interactions detected in *S.*
513 *pombe*, *Drosophila*, and humans support the existence of a conserved complex consisting of
514 PRMT3, RPS2, and PDCD2L. An increasing number of studies suggest functional roles for
515 ribosomal proteins outside of the ribosome (54, 55). Although the extra-ribosomal function of RPS2
516 remains to be determined, its association with proteins that are functionally linked to ribosome
517 biosynthesis, namely PRMT3 and PDCD2L, suggests that the extra-ribosomal role of RPS2 will be
518 related to the regulation of ribosome biogenesis, which appears to be the case for many of the
519 extra-ribosomal functions of ribosomal proteins (56).

520

PDCD2L contributes to small ribosomal subunit biogenesis

522 In addition to the identification of a complex between PDCD2L, RPS2, and PRMT3, our study
523 suggests that a fraction of PDCD2L escorts late precursors of the 40S ribosomal subunit to the
524 cytoplasm. The conclusion that PDCD2L physically associates with pre-40S ribosomal particles is

525 supported by several observations: (i) SILAC-based proteomic analysis of PDCD2L-associated
526 proteins identified several maturation factors found in late pre-40S ribosomal particles, including
527 hRRP12, hLTV1, PNO1, Bystin, NOC4L, and C21orf70 (**Fig. 3A-3B**); (ii) immunoprecipitates of
528 PDCD2L were preferentially enriched for ribosomal proteins of the 40S subunit relative to 60S
529 subunit (**Fig. S2**); (iii) PDCD2L co-sedimented with 40S/pre-40S particles on sucrose gradients
530 (**Fig. 3C**), and (iv) PDCD2L-bound 40S particles were enriched for 18S-E pre-rRNA (**Fig. 3E-3F**),
531 the last precursor to mature 18S rRNA. Important to this study is also the demonstration that
532 PDCD2L actively shuttles between the nucleus and the cytoplasm via binding to the major cellular
533 exportin, CRM1, using a leucine-rich nuclear export signal (NES) (**Fig. 4**). Accordingly, the
534 association of PDCD2L with pre-40S particles, together with the ability of PDCD2L to rapidly export
535 the nucleus via a direct interaction with CRM1, suggest a model in which PDCD2L serves as an
536 adaptor protein for CRM1-mediated export of pre-40S particles. In this model, nucleolar PDCD2L
537 (**Fig. 5**) would be recruited to 40S precursors via interactions with RPS2, a late-associating
538 ribosomal protein that has been shown to be important for the nuclear export of pre-40S subunits
539 (57-59). The leucine-rich NES of PDCD2L could then recruit CRM1 to nuclear pre-40S particles to
540 stimulate transit through the nuclear pore complex to the cytoplasm. However, our data revealed
541 that PDCD2L is not absolutely required for export of 40S precursors in HeLa cells, as *PDCD2L*-null
542 cells are viable and do not show a global retention of pre-40S particles in the nucleus.

543 In contrast to steady state RNA analyses and fluorescent in situ hybridization (FISH)
544 assays, which may not readily detect a modest reduction in the biogenesis and function of
545 ribosomes, ribosome profiles by sucrose gradient sedimentation can provide a highly sensitive
546 assay, as ribosomes are analyzed as free subunits, single monosomes, and polysomes. Since 5-
547 10% of the ribosomal subunits are not assembled into ribosomes (60, 61), a slight deficiency in
548 ribosomal subunit availability can result in a detectable change in the ratio between free ribosomal
549 subunits, which may not be detected on the whole ribosome population. Accordingly, despite the
550 absence of noticeable changes in monosome and polysome distributions, analysis of ribosome
551 profiles using extracts from *PDCD2L*-null cells revealed the accumulation of free 60S ribosomal
552 subunits. Such accumulations of free 60S subunits are generally the consequence of alteration in
553 40S subunit production as a result of a deficiency in a factor that promotes small subunit
554 biogenesis (21, 35, 62-64). Consistent with this view, depletion of the putative homolog of PDCD2L
555 in *S. cerevisiae*, *Tsr4p*, results in a striking accumulation of free 60S subunit together with reduced
556 levels of free 40S ribosomal subunits (29). Intriguingly, the accumulation of free 60S subunits
557 detected in *PDCD2L*-null cells was not accompanied by an apparent decrease in the levels of free
558 40S ribosomal subunits. Although the core features of ribosome assembly are similar from yeast to

Landry-Voyer et al., 2016

559 humans and several proteins involved in the biogenesis of 40S subunits are evolutionarily
560 conserved, data suggest that ribosome biogenesis has increased in complexity and flexibility
561 during the course of evolution (65, 66). Accordingly, whereas the *TSR4* gene is indispensable for
562 budding yeast viability, our data indicate that PDCD2L is not essential in HeLa cells, suggesting
563 the presence of redundant factors that can compensate for the absence of PDCD2L in mammalian
564 cells or the acquisition of a specialized function.

565 One potential candidate that could compensate for small ribosomal subunit production in
566 the absence of PDCD2L is its paralog, PDCD2. Indeed, the synergistic defect in 60S subunit
567 accumulation in cells deficient for both PDCD2L and PDCD2 (**Fig. 8**) suggest functional
568 redundancy between the two paralogs. Moreover, our data indicate that both PDCD2 and PDCD2L
569 form a complex with RPS2 and PRMT3; yet, they appear to form two independent complexes as
570 PDCD2L was not detected in the PDCD2 purification, and reciprocally, PDCD2 was not identified
571 as a PDCD2L-associated protein. Members of a duplicate gene pair can follow different fates after
572 a duplication event. For instance, one paralog might accumulate mutations and evolve a new
573 function, whereas the other paralog retains its ancestral function; alternatively, mutations in both
574 paralogous genes can lead to a partitioning of their ancestral function (67). PDCD2L and PDCD2
575 belong to a family of proteins containing a TYPP (*Tsr4*, *YwqG*, *PDCD2L*, *PDCD2*) domain, which
576 was interrupted by the insertion of a MYND zinc finger domain in PDCD2 (28). It is probable that
577 the insertion of a MYND domain in PDCD2 allowed the acquisition of new functions, which may
578 explain the lack of overlap between the protein interaction networks of PDCD2 and PDCD2L, with
579 the exception of RPS2 and PRMT3. We therefore speculate that PDCD2L and PDCD2 contribute
580 to 40S ribosomal subunit production via parallel pathways that converge to the RPS2-PRMT3
581 complex.

582 The exact mechanism underlying PDCD2L-dependent accumulation of free 60S subunits
583 still needs investigation, but may include possible influences on the export of pre-40S particles. We
584 see at least two plausible scenarios that could explain the accumulation of free 60S subunit without
585 apparent changes in the levels of 40S subunits in *PDCD2L*-null cells: (i) PDCD2L functions as one
586 of several redundant adaptors that promote CRM1-mediated nuclear export of pre-40S particles or
587 (ii) PDCD2L contributes to the export and/or maturation of a sub-population of 40S ribosomal
588 particle that is involved in a specialized function. The first possibility is supported by evidence
589 showing that Rio2, a conserved ribosome biogenesis factor that binds directly to CRM1 and
590 associates with 40S precursors, promotes pre-40S export in yeast and humans (42, 68). Ltv1p and
591 Dim2p, which are the homologs of mammalian hLTV1 and hDIM2/PNO1, respectively, have also
592 been shown to promote pre-40S export in *S. cerevisiae* and were suggested as possible adaptors

Landry-Voyer et al., 2016

593 for CRM1-mediated export of 40S precursors (69, 70). Evidence in yeast also indicates that the
594 conserved Mex67-Mtr2 complex can facilitate nuclear export of pre-40S particles (71) and that
595 Rrp12p binds to pre-rRNA to promote export of ribosomal subunits (72). It is therefore likely that
596 redundant pre-40S export adaptors allow sufficient pre-40S export in the absence of PDCD2L to
597 cause only minimal perturbations in 40S availability in the cytoplasm of *PDCD2L*-null cells.
598 Consistent with the activation of compensatory pathways, we found *trans*-acting factors involved in
599 the late stages of 40S subunit maturation to be up-regulated in *PDCD2L*-null cells (**Fig. S7**).

600 In summary, we provide evidence for the existence of an evolutionarily conserved extra-
601 ribosomal complex that includes PDCD2L, RPS2, and PRMT3. Furthermore, our functional
602 characterization of human PDCD2L suggest a role in small subunit biogenesis, possibly acting as
603 an adaptor protein for CRM1-dependent nuclear export of pre-40S particles. Given that PDCD2L
604 appears to contribute to cell cycle progression and cell proliferation in humans (73) and *Drosophila*
605 (74, 75), elucidating the cellular functions of PDCD2L should provide significant insights into the
606 mechanisms that coordinate ribosome biogenesis and cellular proliferation.

607

608

ACKNOWLEDGMENTS

609 We are grateful to Mark Bedford for generously sharing the RPS2 antibody and to Marlene
610 Oeffinger for critical reading of the manuscript. This work was supported by the Canadian Institutes
611 of Health Research grant MOP-273292 to F.B. and by a graduate scholarship from the Natural
612 Sciences and Engineering Research Council of Canada to A-M.L-V.. F.B. is a Canada Research
613 Chair in the Quality Control of Gene Expression.

614

615

REFERENCES

- 616 1. **Woolford JL, Jr., Baserga SJ.** 2013. Ribosome biogenesis in the yeast *Saccharomyces*
617 *cerevisiae*. *Genetics* **195**:643-681.
- 618 2. **Kusnadi EP, Hannan KM, Hicks RJ, Hannan RD, Pearson RB, Kang J.** 2015. Regulation of
619 rDNA transcription in response to growth factors, nutrients and energy. *Gene* **556**:27-34.
- 620 3. **Sanchez CG, Teixeira FK, Czech B, Preall JB, Zamparini AL, Seifert JR, Malone CD,**
621 **Hannon GJ, Lehmann R.** 2016. Regulation of Ribosome Biogenesis and Protein Synthesis
622 Controls Germline Stem Cell Differentiation. *Cell Stem Cell* **18**:276-290.
- 623 4. **Zhang Q, Shalaby NA, Buszczak M.** 2014. Changes in rRNA transcription influence
624 proliferation and cell fate within a stem cell lineage. *Science* **343**:298-301.
- 625 5. **Gentilella A, Kozma SC, Thomas G.** 2015. A liaison between mTOR signaling, ribosome
626 biogenesis and cancer. *Biochim Biophys Acta* **1849**:812-820.
- 627 6. **Henras AK, Plisson-Chastang C, O'Donohue MF, Chakraborty A, Gleizes PE.** 2015. An
628 overview of pre-ribosomal RNA processing in eukaryotes. *Wiley Interdiscip Rev RNA*
629 **6**:225-242.
- 630 7. **Nerurkar P, Altvater M, Gerhardy S, Schutz S, Fischer U, Weirich C, Panse VG.** 2015.
631 Eukaryotic Ribosome Assembly and Nuclear Export. *Int Rev Cell Mol Biol* **319**:107-140.
- 632 8. **Gadal O, Strauss D, Kessl J, Trumpower B, Tollervey D, Hurt E.** 2001. Nuclear export of
633 60s ribosomal subunits depends on Xpo1p and requires a nuclear export sequence-
634 containing factor, Nmd3p, that associates with the large subunit protein Rpl10p. *Mol Cell*
635 *Biol* **21**:3405-3415.
- 636 9. **Ho JH, Kallstrom G, Johnson AW.** 2000. Nmd3p is a Crm1p-dependent adapter protein for
637 nuclear export of the large ribosomal subunit. *J Cell Biol* **151**:1057-1066.
- 638 10. **Thomas F, Kutay U.** 2003. Biogenesis and nuclear export of ribosomal subunits in higher
639 eukaryotes depend on the CRM1 export pathway. *J Cell Sci* **116**:2409-2419.
- 640 11. **Trotta CR, Lund E, Kahan L, Johnson AW, Dahlberg JE.** 2003. Coordinated nuclear export
641 of 60S ribosomal subunits and NMD3 in vertebrates. *Embo J* **22**:2841-2851.
- 642 12. **Xue S, Barna M.** 2012. Specialized ribosomes: a new frontier in gene regulation and
643 organismal biology. *Nat Rev Mol Cell Biol* **13**:355-369.
- 644 13. **Lee SW, Berger SJ, Martinovic S, Pasa-Tolic L, Anderson GA, Shen Y, Zhao R, Smith RD.**
645 2002. Direct mass spectrometric analysis of intact proteins of the yeast large ribosomal
646 subunit using capillary LC/FTICR. *Proc Natl Acad Sci U S A* **99**:5942-5947.
- 647 14. **Louie DF, Resing KA, Lewis TS, Ahn NG.** 1996. Mass spectrometric analysis of 40 S
648 ribosomal proteins from Rat-1 fibroblasts. *J Biol Chem* **271**:28189-28198.
- 649 15. **Odintsova TI, Muller EC, Ivanov AV, Egorov TA, Bienert R, Vladimirov SN, Kostka S,**
650 **Otto A, Wittmann-Liebold B, Karpova GG.** 2003. Characterization and analysis of
651 posttranslational modifications of the human large cytoplasmic ribosomal subunit proteins
652 by mass spectrometry and Edman sequencing. *J Protein Chem* **22**:249-258.

Landry-Voyer et al., 2016

- 653 16. **Kruiswijk T, Kunst A, Planta RJ, Mager WH.** 1978. Modification of yeast ribosomal
654 proteins. Methylation. *Biochem J* **175**:221-225.
- 655 17. **Lhoest J, Lobet Y, Costers E, Colson C.** 1984. Methylated proteins and amino acids in the
656 ribosomes of *Saccharomyces cerevisiae*. *Eur J Biochem* **141**:585-590.
- 657 18. **Ramagopal S.** 1991. Covalent modifications of ribosomal proteins in growing and
658 aggregation-competent *dictyostelium discoideum*: phosphorylation and methylation.
659 *Biochem Cell Biol* **69**:263-268.
- 660 19. **Chang FN, Navickas IJ, Au C, Budzilowicz C.** 1978. Identification of the methylated
661 ribosomal proteins in HeLa cells and the fluctuation of methylation during the cell cycle.
662 *Biochim Biophys Acta* **518**:89-94.
- 663 20. **Yu Y, Ji H, Doudna JA, Leary JA.** 2005. Mass spectrometric analysis of the human 40S
664 ribosomal subunit: native and HCV IRES-bound complexes. *Protein Sci* **14**:1438-1446.
- 665 21. **Bachand F, Silver PA.** 2004. PRMT3 is a ribosomal protein methyltransferase that affects
666 the cellular levels of ribosomal subunits. *Embo J* **23**:2641-2650.
- 667 22. **Bachand F.** 2007. Protein Arginine Methyltransferases: from Unicellular Eukaryotes to
668 Humans. *Eukaryot Cell*.
- 669 23. **Perreault A, Gascon S, D'Amours A, Aletta JM, Bachand F.** 2009. A methyltransferase-
670 independent function for Rmt3 in ribosomal subunit homeostasis. *J Biol Chem* **284**:15026-
671 15037.
- 672 24. **Swiercz R, Person MD, Bedford MT.** 2005. Ribosomal protein S2 is a substrate for
673 mammalian PRMT3 (protein arginine methyltransferase 3). *Biochem J* **386**:85-91.
- 674 25. **Lipson RS, Webb KJ, Clarke SG.** 2010. Rmt1 catalyzes zinc-finger independent arginine
675 methylation of ribosomal protein Rps2 in *Saccharomyces cerevisiae*. *Biochem Biophys Res*
676 *Commun* **391**:1658-1662.
- 677 26. **Hang R, Liu C, Ahmad A, Zhang Y, Lu F, Cao X.** 2014. Arabidopsis protein arginine
678 methyltransferase 3 is required for ribosome biogenesis by affecting precursor ribosomal
679 RNA processing. *Proc Natl Acad Sci U S A* **111**:16190-16195.
- 680 27. **Swiercz R, Cheng D, Kim D, Bedford MT.** 2007. Ribosomal protein rpS2 is
681 hypomethylated in PRMT3-deficient mice. *J Biol Chem* **282**:16917-16923.
- 682 28. **Burroughs AM, Aravind L.** 2014. Analysis of two domains with novel RNA-processing
683 activities throws light on the complex evolution of ribosomal RNA biogenesis. *Front Genet*
684 **5**:424.
- 685 29. **Li Z, Lee I, Moradi E, Hung NJ, Johnson AW, Marcotte EM.** 2009. Rational extension of the
686 ribosome biogenesis pathway using network-guided genetics. *PLoS Biol* **7**:e1000213.
- 687 30. **Bergeron D, Pal G, Beaulieu YB, Chabot B, Bachand F.** 2015. Regulated Intron Retention
688 and Nuclear Pre-mRNA Decay Contribute to PABPN1 Autoregulation. *Mol Cell Biol*
689 **35**:2503-2517.
- 690 31. **Ran FA, Hsu PD, Wright J, Agarwala V, Scott DA, Zhang F.** 2013. Genome engineering
691 using the CRISPR-Cas9 system. *Nat Protoc* **8**:2281-2308.
- 692 32. **Drissi R, Dubois ML, Douziech M, Boisvert FM.** 2015. Quantitative Proteomics Reveals
693 Dynamic Interactions of the Minichromosome Maintenance Complex (MCM) in the Cellular
694 Response to Etoposide Induced DNA Damage. *Mol Cell Proteomics* **14**:2002-2013.
- 695 33. **Bachand F, Yao XJ, Hrimech M, Rougeau N, Cohen EA.** 1999. Incorporation of Vpr into
696 human immunodeficiency virus type 1 requires a direct interaction with the p6 domain of
697 the p55 gag precursor. *J Biol Chem* **274**:9083-9091.
- 698 34. **Carron C, O'Donohue MF, Choessel V, Faubladiet M, Gleizes PE.** 2011. Analysis of two
699 human pre-ribosomal factors, bystin and hTsr1, highlights differences in evolution of
700 ribosome biogenesis between yeast and mammals. *Nucleic Acids Res* **39**:280-291.

- 701 35. **Choemmel V, Fribourg S, Aguisa-Toure AH, Pinaud N, Legrand P, Gazda HT, Gleizes**
702 **PE.** 2008. Mutation of ribosomal protein RPS24 in Diamond-Blackfan anemia results in a
703 ribosome biogenesis disorder. *Hum Mol Genet* **17**:1253-1263.
- 704 36. **Mallet PL, Bachand F.** 2013. A proline-tyrosine nuclear localization signal (PY-NLS) is
705 required for the nuclear import of fission yeast PAB2, but not of human PABPN1. *Traffic*
706 **14**:282-294.
- 707 37. **Port SA, Monecke T, Dickmanns A, Spillner C, Hofele R, Urlaub H, Ficner R,**
708 **Kehlenbach RH.** 2015. Structural and Functional Characterization of CRM1-Nup214
709 Interactions Reveals Multiple FG-Binding Sites Involved in Nuclear Export. *Cell Rep*
710 **13**:690-702.
- 711 38. **Ong SE, Blagoev B, Kratchmarova I, Kristensen DB, Steen H, Pandey A, Mann M.** 2002.
712 Stable isotope labeling by amino acids in cell culture, SILAC, as a simple and accurate
713 approach to expression proteomics. *Mol Cell Proteomics* **1**:376-386.
- 714 39. **Giot L, Bader JS, Brouwer C, Chaudhuri A, Kuang B, Li Y, Hao YL, Ooi CE, Godwin B,**
715 **Vitols E, Vijayadamodar G, Pochart P, Machineni H, Welsh M, Kong Y, Zerhusen B,**
716 **Malcolm R, Varrone Z, Collis A, Minto M, Burgess S, McDaniel L, Stimpson E, Spriggs F,**
717 **Williams J, Neurath K, Ioime N, Agee M, Voss E, Furtak K, Renzulli R, Aanensen N,**
718 **Carrolla S, Bickelhaupt E, Lazovatsky Y, DaSilva A, Zhong J, Stanyon CA, Finley RL, Jr.,**
719 **White KP, Braverman M, Jarvie T, Gold S, Leach M, Knight J, Shimkets RA, McKenna**
720 **MP, Chant J, Rothberg JM.** 2003. A Protein Interaction Map of *Drosophila melanogaster*.
721 *Science* **302**:1727-1736.
- 722 40. **Schafer T, Strauss D, Petfalski E, Tollervey D, Hurt E.** 2003. The path from nucleolar 90S
723 to cytoplasmic 40S pre-ribosomes. *Embo J* **22**:1370-1380.
- 724 41. **Wyler E, Zimmermann M, Widmann B, Gstaiger M, Pfannstiel J, Kutay U, Zemp I.** 2011.
725 Tandem affinity purification combined with inducible shRNA expression as a tool to study
726 the maturation of macromolecular assemblies. *RNA* **17**:189-200.
- 727 42. **Zemp I, Wild T, O'Donohue MF, Wandrey F, Widmann B, Gleizes PE, Kutay U.** 2009.
728 Distinct cytoplasmic maturation steps of 40S ribosomal subunit precursors require hRio2. *J*
729 *Cell Biol* **185**:1167-1180.
- 730 43. **Rouquette J, Choemmel V, Gleizes PE.** 2005. Nuclear export and cytoplasmic processing of
731 precursors to the 40S ribosomal subunits in mammalian cells. *Embo J* **24**:2862-2872.
- 732 44. **Kirli K, Karaca S, Dehne HJ, Samwer M, Pan KT, Lenz C, Urlaub H, Gorlich D.** 2015. A
733 deep proteomics perspective on CRM1-mediated nuclear export and nucleocytoplasmic
734 partitioning. *Elife* **4**.
- 735 45. **Thakar K, Karaca S, Port SA, Urlaub H, Kehlenbach RH.** 2013. Identification of CRM1-
736 dependent Nuclear Export Cargos Using Quantitative Mass Spectrometry. *Mol Cell*
737 *Proteomics* **12**:664-678.
- 738 46. **Kudo N, Matsumori N, Taoka H, Fujiwara D, Schreiner EP, Wolff B, Yoshida M,**
739 **Horinouchi S.** 1999. Leptomycin B inactivates CRM1/exportin 1 by covalent modification
740 at a cysteine residue in the central conserved region. *Proc Natl Acad Sci U S A* **96**:9112-
741 9117.
- 742 47. **Fu SC, Imai K, Horton P.** 2011. Prediction of leucine-rich nuclear export signal containing
743 proteins with NESsential. *Nucleic Acids Res* **39**:e111.
- 744 48. **la Cour T, Kiemer L, Molgaard A, Gupta R, Skriver K, Brunak S.** 2004. Analysis and
745 prediction of leucine-rich nuclear export signals. *Protein Eng Des Sel* **17**:527-536.
- 746 49. **Kutay U, Guttinger S.** 2005. Leucine-rich nuclear-export signals: born to be weak. *Trends*
747 *Cell Biol* **15**:121-124.

- 748 50. **Meyer BE, Malim MH.** 1994. The HIV-1 Rev trans-activator shuttles between the nucleus
749 and the cytoplasm. *Genes Dev* **8**:1538-1547.
- 750 51. **Boisvert FM, Lam YW, Lamont D, Lamond AI.** 2010. A quantitative proteomics analysis of
751 subcellular proteome localization and changes induced by DNA damage. *Mol Cell*
752 *Proteomics* **9**:457-470.
- 753 52. **Minakhina S, Naryshkina T, Changela N, Tan W, Steward R.** 2016. Zfrp8/PDCD2
754 Interacts with RpS2 Connecting Ribosome Maturation and Gene-Specific Translation. *PLoS*
755 *One* **11**:e0147631.
- 756 53. **Huttlin EL, Ting L, Bruckner RJ, Gebreab F, Gygi MP, Szpyt J, Tam S, Zarraga G, Colby**
757 **G, Baltier K, Dong R, Guarani V, Vaites LP, Ordureau A, Rad R, Erickson BK, Wuhr M,**
758 **Chick J, Zhai B, Kolippakkam D, Mintseris J, Obar RA, Harris T, Artavanis-Tsakonas S,**
759 **Sowa ME, De Camilli P, Paulo JA, Harper JW, Gygi SP.** 2015. The BioPlex Network: A
760 Systematic Exploration of the Human Interactome. *Cell* **162**:425-440.
- 761 54. **Bhavsar RB, Makley LN, Tsonis PA.** 2010. The other lives of ribosomal proteins. *Hum*
762 *Genomics* **4**:327-344.
- 763 55. **Lu H, Zhu YF, Xiong J, Wang R, Jia Z.** 2015. Potential extra-ribosomal functions of
764 ribosomal proteins in *Saccharomyces cerevisiae*. *Microbiol Res* **177**:28-33.
- 765 56. **Warner JR, McIntosh KB.** 2009. How common are extraribosomal functions of ribosomal
766 proteins? *Mol Cell* **34**:3-11.
- 767 57. **Ferreira-Cerca S, Poll G, Gleizes PE, Tschochner H, Milkereit P.** 2005. Roles of
768 eukaryotic ribosomal proteins in maturation and transport of pre-18S rRNA and ribosome
769 function. *Mol Cell* **20**:263-275.
- 770 58. **O'Donohue MF, Choemel V, Faubladiet M, Fichant G, Gleizes PE.** 2010. Functional
771 dichotomy of ribosomal proteins during the synthesis of mammalian 40S ribosomal
772 subunits. *J Cell Biol* **190**:853-866.
- 773 59. **Perreault A, Bellemer C, Bachand F.** 2008. Nuclear export competence of pre-40S
774 subunits in fission yeast requires the ribosomal protein Rps2. *Nucleic Acids Res* **36**:6132-
775 6142.
- 776 60. **Moy TI, Silver PA.** 2002. Requirements for the nuclear export of the small ribosomal
777 subunit. *J Cell Sci* **115**:2985-2995.
- 778 61. **Sivan G, Kedersha N, Elroy-Stein O.** 2007. Ribosomal slowdown mediates translational
779 arrest during cellular division. *Mol Cell Biol* **27**:6639-6646.
- 780 62. **Fassio CA, Schofield BJ, Seiser RM, Johnson AW, Lycan DE.** 2010. Dominant mutations in
781 the late 40S biogenesis factor Ltv1 affect cytoplasmic maturation of the small ribosomal
782 subunit in *Saccharomyces cerevisiae*. *Genetics* **185**:199-209.
- 783 63. **Kressler D, de la Cruz J, Rojo M, Linder P.** 1997. Fal1p is an essential DEAD-box protein
784 involved in 40S-ribosomal-subunit biogenesis in *Saccharomyces cerevisiae*. *Mol Cell Biol*
785 **17**:7283-7294.
- 786 64. **Ounap K, Kasper L, Kurg A, Kurg R.** 2013. The human WBSCR22 protein is involved in the
787 biogenesis of the 40S ribosomal subunits in mammalian cells. *PLoS One* **8**:e75686.
- 788 65. **Lafontaine DL.** 2015. Noncoding RNAs in eukaryotic ribosome biogenesis and function.
789 *Nat Struct Mol Biol* **22**:11-19.
- 790 66. **Tafforeau L, Zorbas C, Langhendries JL, Mullineux ST, Stamatopoulou V, Mullier R,**
791 **Wacheul L, Lafontaine DL.** 2013. The complexity of human ribosome biogenesis revealed
792 by systematic nucleolar screening of Pre-rRNA processing factors. *Mol Cell* **51**:539-551.
- 793 67. **Perez-Perez JM, Candela H, Micol JL.** 2009. Understanding synergy in genetic
794 interactions. *Trends Genet* **25**:368-376.

Landry-Voyer et al., 2016

- 795 68. **Fischer U, Schauble N, Schutz S, Altvater M, Chang Y, Faza MB, Panse VG.** 2015. A non-
796 canonical mechanism for Crm1-export cargo complex assembly. *Elife* **4**.
797 69. **Seiser RM, Sundberg AE, Wollam BJ, Zobel-Thropp P, Baldwin K, Spector MD, Lycan**
798 **DE.** 2006. Ltv1 is required for efficient nuclear export of the ribosomal small subunit in
799 *Saccharomyces cerevisiae*. *Genetics* **174**:679-691.
800 70. **Vanrobays E, Lepus A, Osheim YN, Beyer AL, Wacheul L, Lafontaine DL.** 2008. TOR
801 regulates the subcellular distribution of DIM2, a KH domain protein required for
802 cotranscriptional ribosome assembly and pre-40S ribosome export. *RNA* **14**:2061-2073.
803 71. **Faza MB, Chang Y, Occhipinti L, Kemmler S, Panse VG.** 2012. Role of Mex67-Mtr2 in the
804 nuclear export of 40S pre-ribosomes. *PLoS Genet* **8**:e1002915.
805 72. **Oeffinger M, Dlakic M, Tollervey D.** 2004. A pre-ribosome-associated HEAT-repeat
806 protein is required for export of both ribosomal subunits. *Genes Dev* **18**:196-209.
807 73. **Chen Q, Yan C, Yan Q, Feng L, Chen J, Qian K.** 2008. The novel MGC13096 protein is
808 correlated with proliferation. *Cell Biochem Funct* **26**:141-145.
809 74. **Bjorklund M, Taipale M, Varjosalo M, Saharinen J, Lahdenpera J, Taipale J.** 2006.
810 Identification of pathways regulating cell size and cell-cycle progression by RNAi. *Nature*
811 **439**:1009-1013.
812 75. **Liang L, Haug JS, Seidel CW, Gibson MC.** 2014. Functional genomic analysis of the
813 periodic transcriptome in the developing *Drosophila* wing. *Dev Cell* **29**:112-127.
814
815
816

817

FIGURES LEGENDS

818 **Figure 1. PDCD2L is a PRMT3-associated protein.** (A) GFP-PRMT3 SILAC copurification results
819 plotted by SILAC ratio out the x-axis (intensity of peptides originating from the GFP-PRMT3
820 purification versus the control purification), which reflects signal specificity; and signal intensity up
821 the y-axis (total peptide intensity for each protein normalized to molecular weight), which reflects
822 the relative abundance of each protein in the purification. Proteins presenting SILAC ratios >2.0
823 and <2.0 are shown as black and white dots, respectively. GFP-PRMT3 (blue), RPS2 (red), and
824 PDCD2L (green) are shown in color. (B) Western analysis of total extracts (Input; lanes 1-4) and
825 anti-Flag precipitates (IP; lanes 5-8) prepared from HEK 293 cells transfected with the empty
826 vector (lanes 2 and 6), Flag-PABPN1 (lanes 3 and 7), and Flag-PDCD2L (lanes 4 and 8)
827 constructs. The asterisk indicates IgG heavy chain. Areas from the same blot were spliced to
828 remove irrelevant lanes (between lanes 3-4 and 7-8). (C) Western blot analysis of
829 immunoprecipitates prepared using a PRMT3-specific antibody (lanes 3-4) and a control IgG
830 antibody (lane 2) using extracts prepared from wild-type (lanes 1-3) and *PDCD2L*-null (1A3; lane 4)
831 cells. The asterisk indicates IgG heavy chain.

832

833 **Figure 2. RPS2 is required for the association between PRMT3 and PDCD2L.** (A) Western
834 analysis of total extracts (lanes 1-2) and anti-Flag immunoprecipitates (lanes 3-4) prepared from
835 HEK 293 cells that stably express Flag-PABPN1 (lanes 1 and 3) and Flag-PDCD2L (lanes 2 and
836 4). The asterisk indicates IgG heavy chain. (B) Analysis of PDCD2L, RPS2, and PRMT3
837 interactions by two-hybrid assay. (i) The LexA and LexA-PDCD2L fusion protein were coexpressed
838 with the full-length VP16-RPS2 fusion. (ii) The LexA, LexA-RPS2, and LexA-PDCD2L proteins
839 were coexpressed with the full-length VP16-PRMT3. Protein interactions were measured using
840 liquid β -galactosidase assays in the *S. cerevisiae* L40 strain and reported as Miller units. Data and
841 error bars represent the mean and standard deviation from three independent experiments using
842 two independent transformants. (C) Western analysis of total extracts (lanes 1-3) and GFP
843 immunoprecipitates (lanes 4-6) prepared from HEK 293 cells stably expressing GFP-PABPN1
844 (lanes 1 and 4) and GFP-PRMT3 (lanes 2-3 and 5-6) that were previously treated with RPS2-
845 specific (lanes 3 and 6) and control nontarget (lanes 1-2 and 4-5) siRNAs. (D) Quantification of
846 RPS2 and PDCD2L levels in GFP-PRMT3 immunoprecipitates. RPS2 and PDCD2L co-purification
847 levels (normalized to GFP-PRMT3) were set to 1.0 for cells treated with control nontarget siRNAs.
848 Data and error bars represent the mean and standard deviation from four independent
849 experiments. ****, $P < 0.0001$; Student's *t* test. (E) Western analysis of total extracts (lanes 1-4)
850 and Flag immunoprecipitates (lanes 5-8) prepared from HEK 293 cells stably expressing Flag-

Landry-Voyer et al., 2016

851 PDCD2L (lanes 3-4 and 7-8) and the empty vector control (lanes 1-2 and 5-6) that were previously
852 treated with PRMT3-specific (lanes 2, 4, 6, and 8) and control nontarget (lanes 1, 3, 5, and 7)
853 siRNAs.

854

855 **Figure 3. PDCD2L associates with late 40S precursors.** (A) GFP-PDCD2L SILAC copurification
856 results plotted by SILAC ratio out the *x*-axis (intensity of peptides originating from the GFP-
857 PDCD2L purification versus the control purification), which reflects signal specificity; and signal
858 intensity up the *y*-axis (total peptide intensity for each protein normalized to molecular weight),
859 which reflects the relative abundance of each protein in the purification. Proteins presenting SILAC
860 ratios >2.0 and <2.0 are shown as black and white dots, respectively. Factors known to be
861 associated with late pre-40S particles are shown in orange. (B) Western analysis of total extracts
862 (lanes 1-2) and Flag immunoprecipitates (lanes 3-4) prepared from HEK 293 cells that stably
863 express Flag-tagged versions of PABPN1 (lanes 1 and 3) and PDCD2L (lanes 2 and 4). (C)
864 Western analysis of endogenous proteins using fractions of centrifuged sucrose gradients that
865 were prepared using extracts of HEK 293 cells. The positions of the 40S, 60S, and 80S
866 sedimentation are indicated at the bottom. (D) Schematic of 18S rRNA biogenesis in human cells.
867 Following cleavage at sites 01/A', A0, 1, and 2, the 21S pre-rRNA is matured into the 18S-E
868 precursor in the nucleus. Final maturation of the 18S-E pre-rRNA into mature 18S rRNA is
869 performed in the cytoplasm. Probes used to detect the 18S-E pre-rRNA (red) as well as mature
870 18S (blue) and 28S (green) rRNAs are indicated. (E) Western (WB, *upper two panels*) and
871 Northern (NB, *lower three panels*) analyses of protein and RNA, respectively, prepared from total
872 cell extracts (lanes 1-2) and Flag immunoprecipitates (lanes 3-4) using HEK 293 cells that stably
873 express Flag-tagged versions of PABPN1 (lanes 1 and 3) and PDCD2L (lanes 2 and 4). The 18S-
874 E, 18S, and 28S RNAs were detected using the specific probes shown in Fig. 3D. (F)
875 Quantification of 18S-E pre-rRNA enrichment. 18S-E levels were normalized to levels of mature
876 18S rRNA. The values were then set to 1.0 for the control Flag-PABPN1 purification. Data and
877 error bars represent the average and standard deviation from three independent experiments.

878

879 **Figure 4. PDCD2L is a nucleo-cytoplasmic shuttling protein that exports the nucleus using a**
880 **leucine-rich nuclear export signal (NES).** (A) U-2 OS cells induced to express GFP-tagged
881 versions of PDCD2L (panels a-f) and PRMT3 (panels g-l) were treated (d-f and j-l) or not treated
882 (a-c and g-i) with leptomycin B (LMB) for 3h. DNA stained with DAPI shows the nucleus of each
883 cell (b, e, h, and k). Scale bar, 20 μ m. (B) Alignment of putative NES of PDCD2L proteins across
884 multicellular organisms. The NES consensus sequence, Φ X₂₋₃ Φ X₂₋₃ Φ X Φ , is indicated on top, where

Landry-Voyer et al., 2016

885 Φ is a large, hydrophobic amino acid and x represents any amino acid. (C) Visual analysis of U-2
886 OS cells that were transiently transfected with DNA constructs expressing GFP-PDCD2L (a-c) and
887 a version of GFP-PDCD2L with substitutions of leucines 162, 165, and 167 to alanines (NESmut,
888 d-f). (D) Visual analysis of U-2 OS cells that were transiently transfected with DNA constructs
889 expressing GFP (a-f) as well as GFP fused to wild-type (g-l) and mutant (m-r) versions of the
890 PDCD2L NES (amino acid 153-181, see Fig. 4E). Cells were treated (+) or not treated (-) with
891 leptomycin B (LMB). (E) Schematic of wild-type and mutant versions GFP-NES-PDCD2L fusions
892 used in Fig. 4D. (F) Direct interaction between PDCD2L and CRM1 *in vitro*. 50 pmol GST, GST-
893 PDCD2L, and GST-Rev fusion proteins were immobilized on beads and incubated with 9 pmol
894 Cy3-labeled CRM1 alone or in the presence of 180 pmol RanGTP_{Q69L} and 70 pmol Nup214₁₉₁₆₋
895 ₂₀₃₃. Bound Cy3-CRM1 was analyzed by flow cytometry and the fluorescence intensity relative to
896 GST was plotted. Data and error bars represent the mean and standard deviation from six
897 independent experiments. *******, $P < 0.001$; ******, $P < 0.01$, Student's *t* test.

898

899 **Figure 5. PDCD2L transits through the nucleolus.** U-2 OS cells conditionally expressing GFP-
900 PDCD2L were treated with leptomycin B (LMB) for 15 min (b, e, h, and k) and 90 min (c, f, i, and l),
901 or left untreated (a, d, g, and j). Fixed cells were simultaneously analyzed by direct GFP
902 fluorescence (g-i) and immunostaining for the nucleolar marker, fibrillarin (d-f). DNA stained with
903 DAPI shows the nucleus of each cell (a-c). Scale bars, 20 μ m.

904

905 **Figure 6. Analysis of pre-rRNA processing in PDCD2L-depleted cells.** (A) Western blot
906 analysis showing depletion of PDCD2L and Bystin from HeLa cells. (B) Northern blot analysis of
907 mature and precursor rRNAs using total RNA prepared from PDCD2L- and Bystin-depleted cells
908 as well as control cells. Pre-rRNAs were detected using a probe complementary to sequences in
909 the 5' internal transcribed spacer (5' ITS, red probe in Fig. 3D) region. Pre-rRNA species are
910 indicated on the left. Areas from the same blot were spliced to remove irrelevant lanes (between
911 lanes 2-3). (C-D) 18S-E (C) and 21S (D) pre-rRNA levels were normalized to the 28S rRNA and
912 expressed relative to cells treated with control siRNA. Data and error bars represent the mean and
913 standard deviation from eight (siBystin) and ten (siPDCD2L) independent experiments. ****** *P*-
914 value < 0.01 , Student's *t*-test.

915

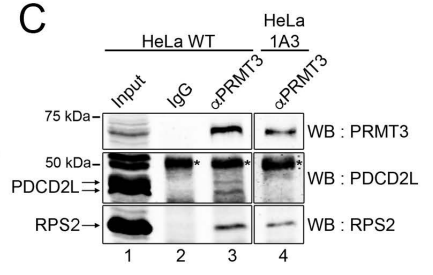
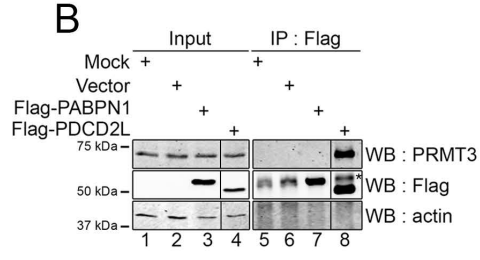
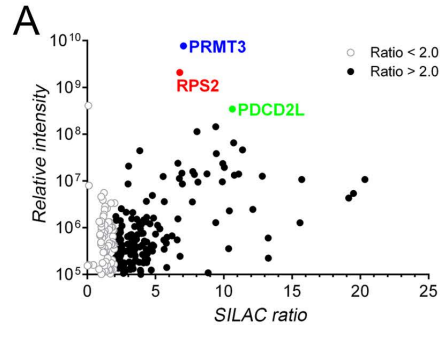
916 **Figure 7. Deletion of PDCD2L causes the accumulation of free 60S ribosomal subunits.** (A)
917 Sucrose gradient analysis of total extracts prepared from wild-type (WT) and *PDCD2L*-null HeLa
918 cells (clones 1A3 and 3B2). The positions of free small (40S) and large (60S) ribosomal subunits,

Landry-Voyer et al., 2016

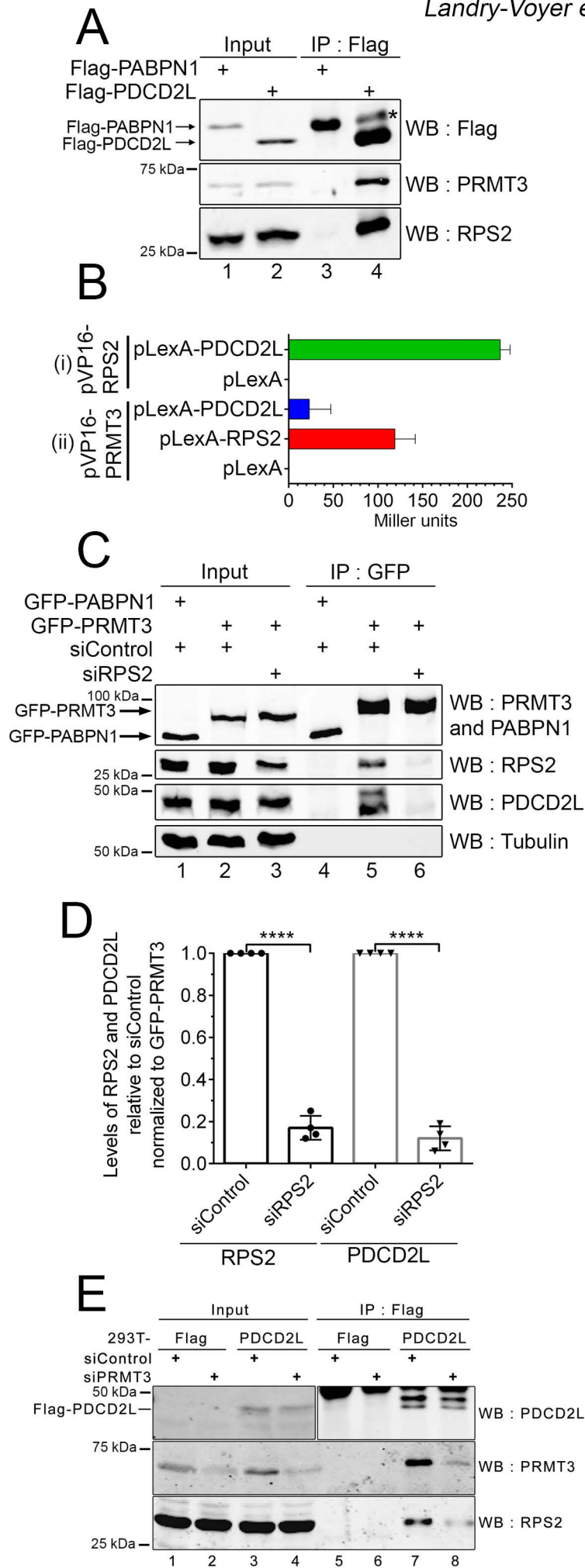
919 monosomes (80S), and polysomes are indicated. (B) Quantification of 60S/40S free ribosomal
920 subunit ratios expressed relative to wild-type HeLa cells. Data and error bars represent the mean
921 and standard deviation from seven (1A3) and six (3B2) independent experiments. (****) *P*-
922 value <0.0001, Student's *t*-test. (C) Sucrose gradient analysis of total extracts prepared from wild-
923 type (WT, panel 1) and PDCD2L-deleted HeLa cells (clone 1A3, panels 2-3) that were previously
924 transfected with an empty vector (EV, panels 1-2) control or a DNA construct expressing Flag-
925 PDCD2L (panel 3). (D) Western blot analysis showing the expression of Flag-PDCD2L in
926 PDCD2L-null cells (lane 3). The band co-migrating with endogenous PDCD2L in lane 3 is a
927 degradation product generated from Flag-PDCD2L.

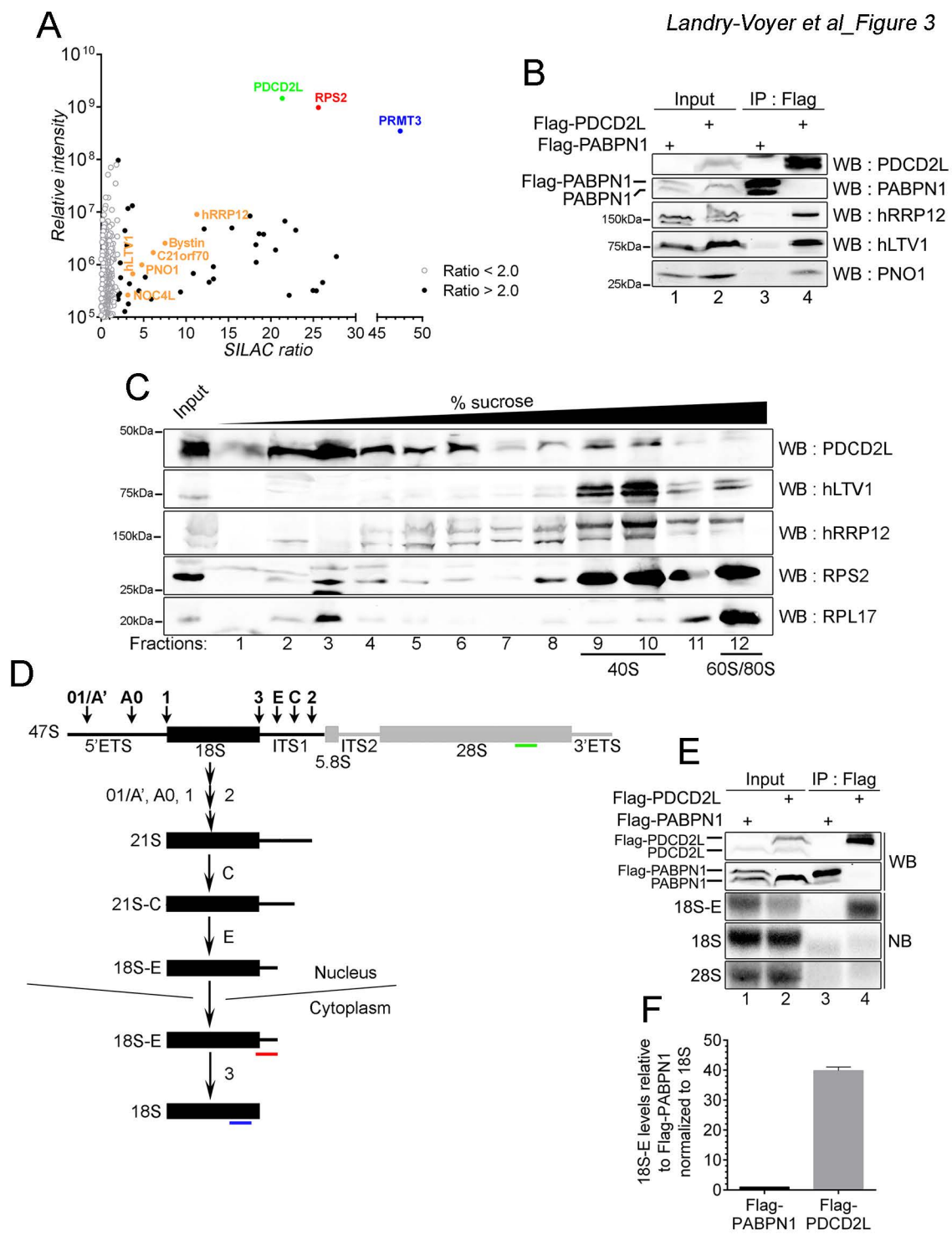
928

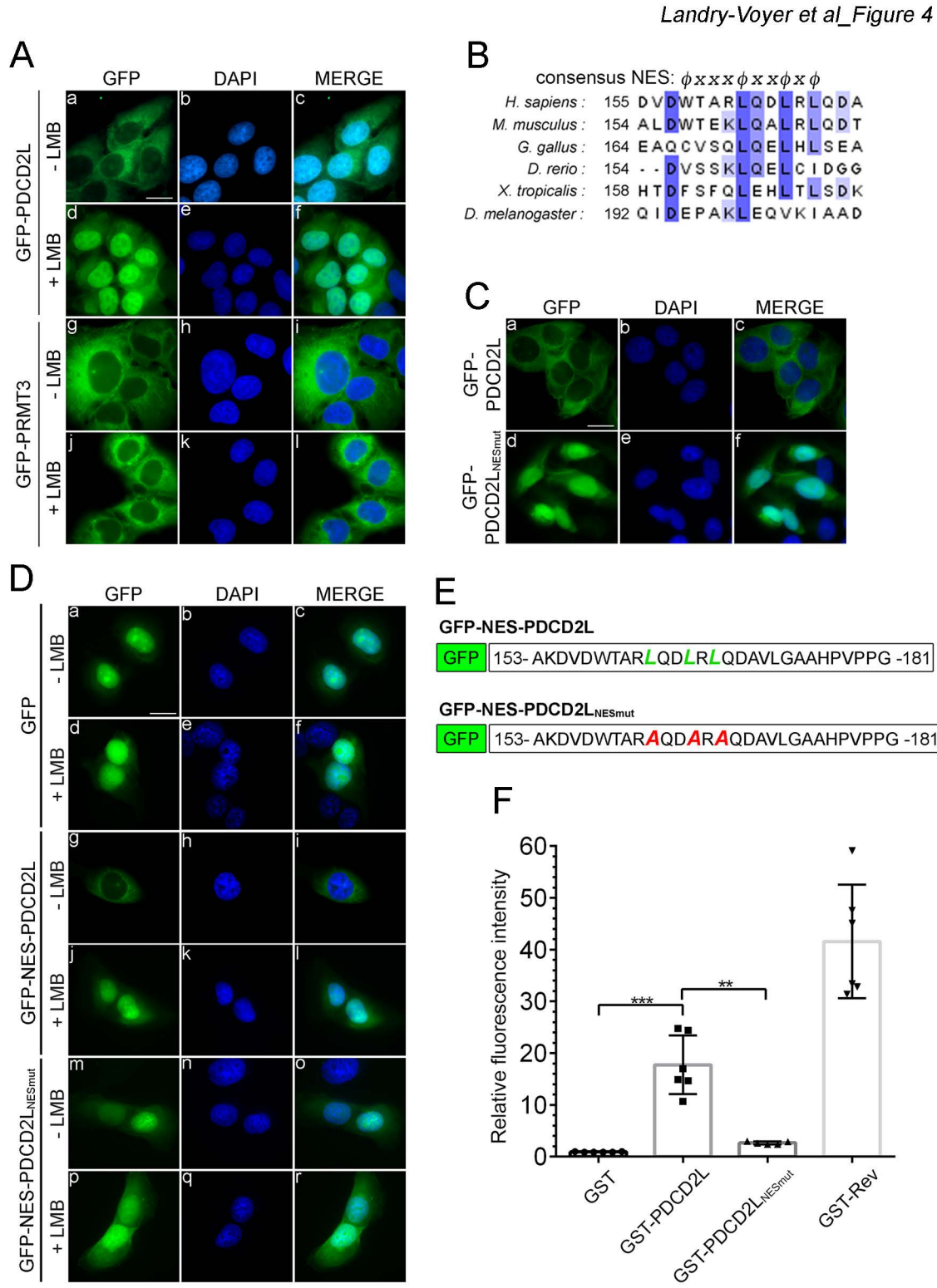
929 **Figure 8. Human PDCD2 and PDCD2L proteins contribute to 40S ribosomal subunit**
930 **production.** (A) Western blot analysis showing depletion of PDCD2 from wild-type HeLa cells
931 (lanes 1-2) as well as PDCD2L-null HeLa cells (1A3; lanes 3-4). (B) Sucrose gradient analysis of
932 total extracts prepared from wild-type (a, b) and PDCD2L-null (c, d) HeLa cells that were previously
933 treated with PDCD2-specific (b and d) or control nontarget (a and c) siRNAs. The positions of free
934 small (40S) and large (60S) ribosomal subunits, monosomes (80S), and polysomes are indicated.
935 (C) Northern blot analysis of mature and precursor rRNAs using total RNA prepared from wild-type
936 (WT; lanes 1-2) and PDCD2L-null (1A3; lanes 3-4) cells that were previously treated with PDCD2-
937 specific (lanes 2 and 4) or control nontarget (lanes 1 and 3) siRNAs. Pre-rRNAs were detected
938 using a probe complementary to sequences in the 5' internal transcribed spacer (5'ITS) region.
939 Pre-rRNA species are indicated on the left. (D-E) 18S-E (D) and 21S (E) pre-rRNA levels were
940 normalized to the 28S rRNA and expressed relative to cells treated with control siRNAs. Data and
941 error bars represent the mean and standard deviation from six independent experiments. (**) *P*-
942 value <0.01, Student's *t*-test. (F) GFP-PDCD2 SILAC copurification results plotted by SILAC ratio
943 out the x-axis and signal intensity up the y-axis. Proteins presenting SILAC ratios >2.0 and <2.0
944 are shown as black and white dots, respectively. GFP-PDCD2 (green), RPS2 (red), and PRMT3
945 (blue) are shown in color.

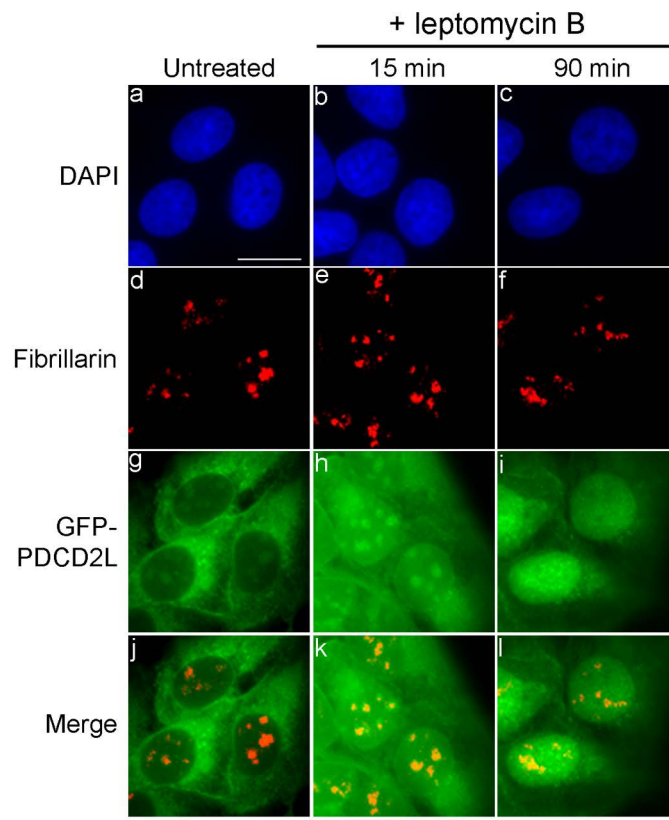


Landry-Voyer et al_Figure 1

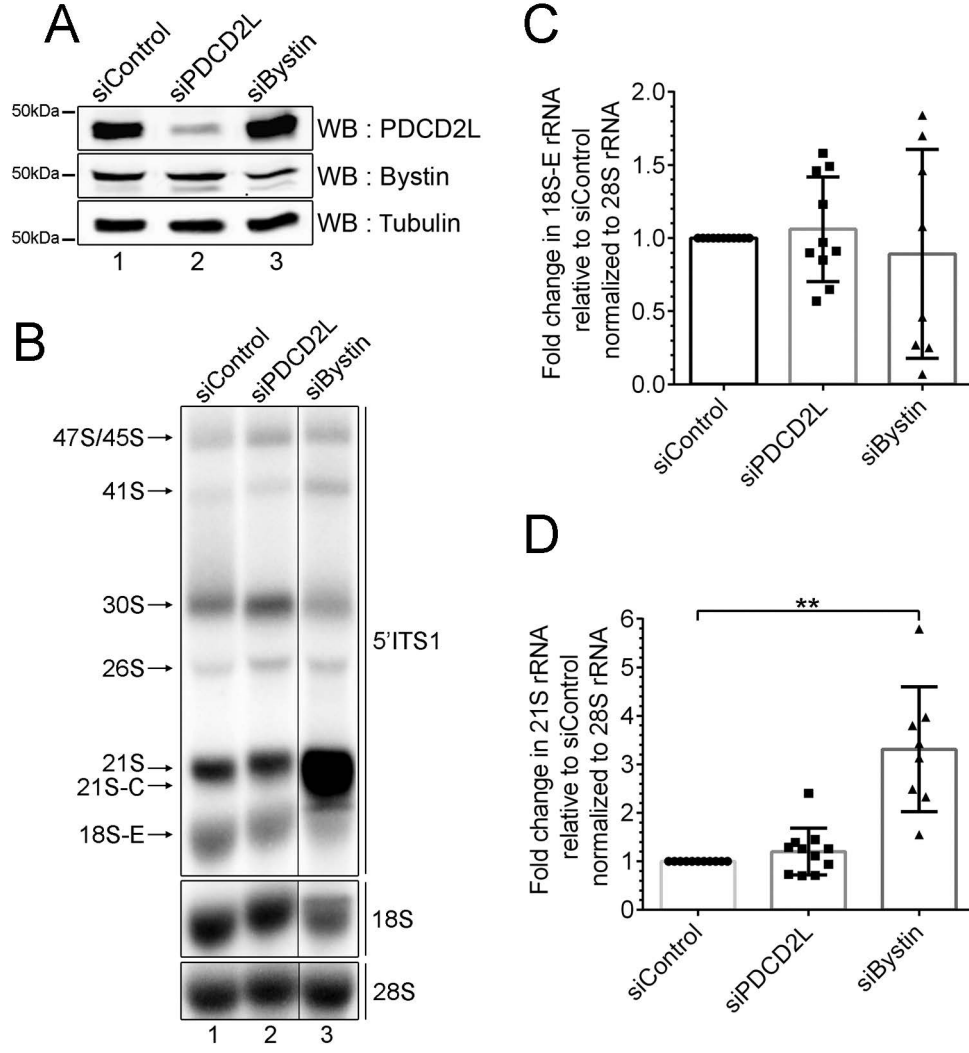


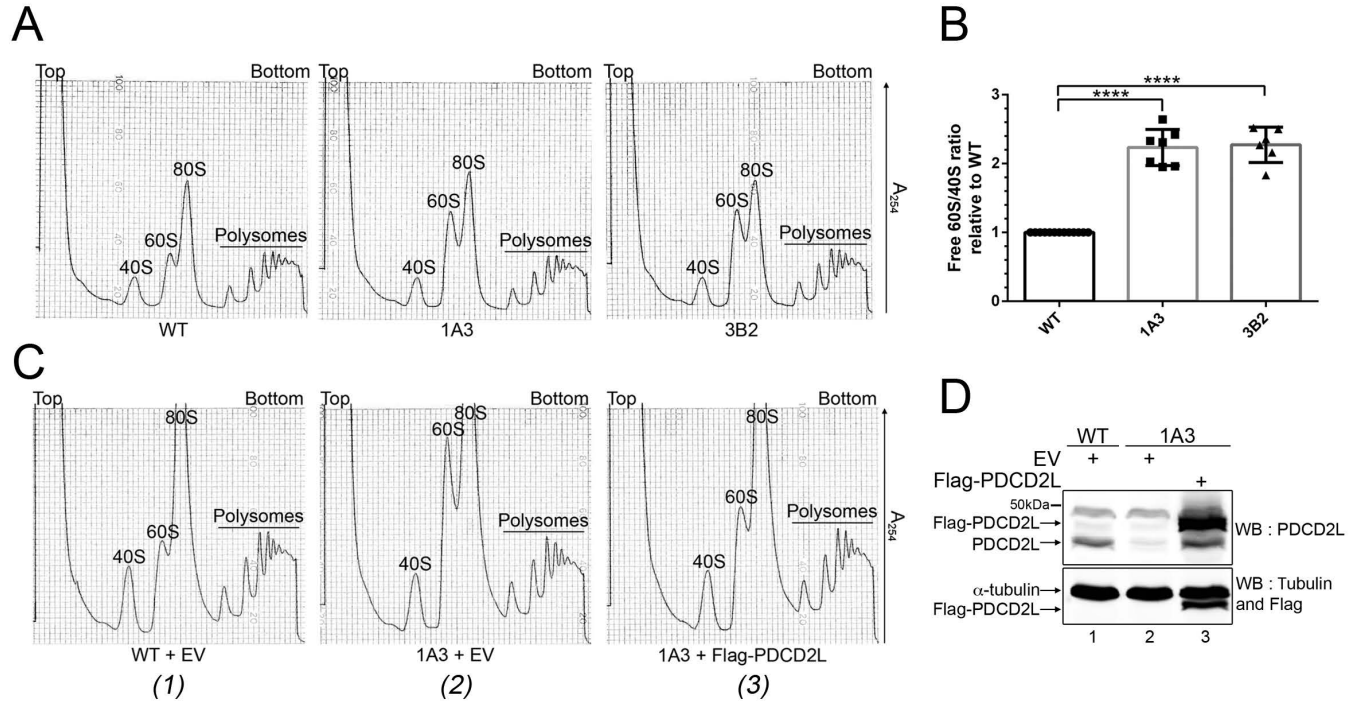




Landry-Voyer et al_Figure 5

Landry-Voyer et al_Figure 6





Landry-Voyer et al_Figure 7

